Draft version November 1, 2018
Typeset using LaTeX default style in AASTeX62

Global and local 3D studies of the residual vector field from 2MASS and Hipparcos-2 catalog

F.J. Marco,[1] M.J. Martínez,[2] and J.A. López[1]

[1] *Universidad Jaume I, Dpt. Matemáticas, IMAC,Castellón, España*
[2] *Universidad Politécnica de Valencia, Dpt. Matemática Aplicada,IUMPA, Valencia, España*

Submitted to PASP

ABSTRACT

Gaia mission will provide a six-parameter solution for millions of stars, including a tridimensional map of our galaxy. The estimation of distances has been made for the TGAS, while to contrast the proper motions it is interesting to consider positions from the different Gaia Data Release with older ones given in ground-based massive catalogs. This process has been followed to build, for example, the PMA catalog using the 2MASS. Our aim is to improve the positions of this catalog, (although the process is applicable to any other) and the first stage, presented here, consists of carrying out a 3D study, using VSH development, of the systematisms in position for the stars common with Hipparcos-2, taking into account the distances, magnitudes and spectral types. To this aim, we use linear polynomial regression of first order that fits vector fields and the derivatives of their components. We verify that the coefficients of the developments of first order have different behavior according to the characteristics of stars and distances.

To deepen the study we focus on the conservative component of the field, applying the Helmholtz theorem. Each potential function is obtained solving a Poisson equation on the sphere, after finding the divergence of the corresponding vector field. Both vector and potential fields present patterns, at certain points, that depend on the three considered parameters (distance, magnitude, and spectral type): their sources and shrinks correspond to maxima and minima. In this sense, we observe that these critical points are also critical points of the surface that represents the VT magnitude of Tycho-2, which makes sense because this catalog was used in the reduction of 2MASS positions. Finally, we selected some stars near the critical points of the vector fields and we apply the adjustments obtained in the previous sections. The difference with the positions in DR1 allows us to compare the proper motions, those from the PMA and those induced after our corrections.

Keywords: Reference systems –Catalogs–Astrometry

1. INTRODUCTION

Astrometry is an astronomical discipline whose objective is to determine positions, parallaxes and proper motions in the most accurate possible way. In the last decades, since Hipparcos mission (that provided Hipparcos and Tycho catalogs (Perryman & ESA 1997)), a much more precise determination for astrometric parameters and, in particular, for parallax was possible than the one obtained using observations from Earth. The uncertainties, taking as reference the improved version - Hipparcos-2 henceforth- by van Leeuwen (van Leeuwen 2007a),(van Leeuwen 2007b) are 0.3 mas for positions and parallaxes and 1 mas / yr for proper motions (data valid for J1991.25). The approximately 120000 stars contained in the catalog are, at best, an order up to 11.5 of H-magnitude. The Hipparcos catalog is the

Corresponding author: F.J. Marco
marco@mat.uji.es

realization of the Hipparcos Celestial Reference Frame (HCRF), which was aligned with the ICRF with the aim of having no system rotation. The estimated error on the expected accuracy of the system rotation of the HCRF with respect to the ICRF was 0.25 mas/yr.

In the frame of the Gaia mission (Prusti et al. 2016), Gaia satellite was launched in 2013 with the objective (see Arenou et al. (2017)), of "measuring the three-dimensional distribution, both in position and in speed, of the stars of our galaxy, as well as the determination of their astrophysical properties." The astrometrical content of the first Gaia Data Release, DR1 (Data Release 1, Lindegren et al. (2016)), consists of two parts: the primary and the secondary data sets. The first of them contains positions, parallax and proper motions for the stars common with the Tycho-2 catalog (Høg et al 2000), obtained by means of the so-called TGAS solution (Michalik el al. 2015). For more details in the precedents of the TGAS construction, see the "Agis paper" (providing an Astrometric Global Iterative Solution Lindegren et al. (2012)) and their application by (Michalik et al. 2014) to obtain the HTPM solution (without using Tycho's stars). For estimated accuracy of TGAS, regarding the 96365 stars common with Hipparcos, the J1991.25 positions have been taken as valid, while the proper motions are estimated to have an accuracy of 0.06 mas/yr and the parallax 0.3 mas (plus another 0.3 mas for a systematic component, see (Brown et al. 2016)). It is very reasonable to expect that these precisions will be improved after the final stage of the 5 years mission (despite having published DR2 in April 2018 (Brown et al. 2018), and other papers included in this special issue, they have not been considered in this paper). This DR1 parallax system is independent of the Hipparcos parallax system, but the comparison carried out by Lindegren et al. (2016)) concludes that the accuracies in both systems are comparable for the Hipparcos stars. Since the publication of DR1, different studies have been carried out on systematic errors, mainly in parallaxes. For instance Stassun K.G. & Torres G., (2016), using 158 eclipsing binary stars and finding some correlations with the ecliptic latitude but not with brightness or color; Zinn et al. (2017), Gontcharov (2017), Davies et al. (2017), Ridder et al. (2016) and Schönrich & Aumer (2017). Also, regarding the proper motions, the PMA catalogue (Akhmetov et al. 2017) has been built from the data of DR1 and a modification of the 2MASS (Cutri et al. 2003), (Skrutskie et al, 2006). These papers, among others, make us think that it may be of interest to consider the use of massive catalogs, (although this mass property it is not necessary: the use of the complete catalog or a subset may be possible, considering the characteristics of our study) to track the consistency/inconsistency in certain parameters measured from different catalogs. In this paper, we have the twofold purpose of study the global and local aspects of the residual 3D vector fields obtained by different comparisons between two astromeric catalogs. More specifically, from the residuals in right ascension and declination, we will consider the discrete three-dimensional vector field associated with these data with the goal of identifying possible systematic differences depending on a set of parameters like magnitudes and spectral types for each fixed distance. On the one hand, we consider Hipparcos-2 van Leeuwen (2007a) with the values of the distances of TGAS, as have been estimated after the studies of (Bailer-Jones 2015) and (Astraatmadja et al. 2016a), (Astraatmadja et al. 2016b). In this sense, it is interesting to note that the measurement of a parallax is a "noisy measure" of the inverse of the distance. Thus, it is only possible to assign a probability to the distance using Bayes Theorem, from parallax observations and an "a piori" distribution of distances in the galaxy. It is precisely in this last article where the catalog of distances for the TGAS catalog is attached. Its existence enables us to carry out a study, with a good precision, in the interval [25; 600] pc, taking slices centered at $r = 100, 200, 300, 400$ and 500 pc in equatorial coordinates, without having to use the inverse of the trigonometrical parallaxes of Hipparcos. A brief comment about this will be made in subsection 2.1. On the other hand, we have chosen as second catalog the 2MASS catalog for two reasons: firstly, because of its use in PPMX Röser et al. (2008) and the PPMXL Röser et al. (2010) position systems and also, because the UCAC4 Zacharias et al. (2013) astrometric reduction was made applying certain corrections in which the 2MASS catalog was used in order to refer to Tycho-2; and, secondly, for being a completely independent catalog from Hipparcos, although the stars of Tycho-2 were used to obtain the reductions. Comparison of the 2MASS point-source positions with the Tycho-2 catalog shows that 2MASS positions are consistent with the ICRS with a net or a set no larger than 15 mas. Similar uncertainty, at best, is achieved for the UCAC4 stars. Some studies about the differences using 2MASS and the UCAC catalogs can be seen in Zacharias et al. (2000), Zacharias et al. (2004) and Zacharias et al. (2013).

Regarding the methods for comparison of catalogs, it is particularly noteworthy that they have been evolving in the last decades because a greater precision in the measurements demands a greater refinement in the theoretical adjustment models. Thus, in the mid-60s of the last century the spherical harmonics were already used in the field of Physical Geodesy (Heiskanen & Moritz 1967). About the same date, Brosche P. (1966) used them for the first time to calculate the systematic part of the residuals obtained by comparing different stellar catalogs (English version

in 1966). This approach allowed the independent development of residuals in AR and DEC. A joint treatment for AR and DEC required the use of vector fields over the sphere and its development, under the hypothesis of regularity (the completeness theorem can be found in Jeffreys (1967)), in vectorial spherical harmonics (VSH henceforth). This method was introduced by Mignard & Morando (1990) in the field aimed at this paper, while an early introduction about the general principles of VSH can be found in the classic Morse & Feshback (1953). This method, applied to the vector fields of residuals both in the projection on the celestial sphere and in different slices, is the one that we apply. In addition, to see how the spectral types and magnitudes affect the results, classifications have been made: a) KM / (Non-KM); b) magnitudes in m4 / m5 / m6 / m7 sets (defined in the article); c) subsets obtained mixing the two previous pure types (KM-m4 to KM-m7 and the same for No-KM). All of them have been studied over the whole sphere and with the spatial subdivision by slices and then the 3D study has been performed, so that the results can be compared in both cases. This part of our work concerns to the Global part of the study. We must mention that the treatment of the data will be carried out through a suitable regression method. More specifically, we use local polynomial regression of first order, fitting the components of the vector fields and the derivatives of these components (it is important to know that we compute estimators for functions and their derivatives, not for the derivatives of the estimator functions). These technical topics will be presented in section 3, after a study of the data in their quantitative (subsection 2.2) and qualitative aspects (subsection 2.3). About the analysis of the vector field of the residuals, we know that the toroidal harmonics correspond to the rotational part of the field and its calculation up to order one can be sufficiently representative. However, this does not happen with the non-rotational part of the vector field. To obtain a more accurate study, we have considered the Helmholtz Theorem which splits each vector field into two components: rotational and non-rotational. This second part coincides with the gradient of a potential function (so, the divergence of the residual field coincides with the Laplacian of such a potential function. See section 4). Thus, it is possible to obtain a high-order development of the potential function in each slice. To calculate both expressions we use local first order polynomial estimators in three dimensions, providing adjustment for the function and its derivatives to calculate the divergence of the vector field. For the second member of the equation we apply the properties of spherical surface harmonics as eigenfunctions of the Laplace- Beltrami operator. The areas of the sphere, for each slice, in which the critical points of the global field and the critical points of the potential are close have no interest from the rotational point of view, but they have interest from the non-rotational point of view. This is the Local part of the work. Once the critical points of the residual vector field for each slice have been related to the critical points of a certain potential function, we have considered the possibility of finding a physical quantity that is relevant in the reduction of data and that may be related to these critical points of the potentials found. In this sense, given that Tycho-2 was the reference chosen in the reduction of positions of the 2MASS stars, we have studied the surfaces determined by the BT and VT magnitudes. It has been checked that in the neighborhood of the critical points of the vector fields the same type of critical point appears on the VT surface (sometimes the BT also behaves the same, but less clearly than the VT. Probably, this is due, or is related, to the fact that this magnitude is closer to the absolute magnitude, but this is merely a speculation) It is interesting to remark that the sources and shrinks (also the saddle points) are patterns that appear depending on the stellar classification carried out (but not necessary in the residual vector field on the whole sphere), while the relative extrema of the surfaces of VT magnitude, appear when we consider all the stars from Tycho-2 in the neighborhood of each point since, obviously, in the process of reduction of the 2MASS did not directly influence the stellar distances. Many results are presented in section 5 and we then we finish in section 6 with a summary of conclusions.

To visualize other possible applications, once the work has been carried out with all the data of the 2MASS in the sense explained above, we have computed some proper motions induced by the corrections obtained in section 5.1 in the neighborhood of some of the singular points of the vector fields presented in 5.2. We proceed to compare the obtained results with those of DR1 and those of the PMA, which, as mentioned, reviewed 2MASS prior to the calculation of its proper motions.

2. PREVIOUS STUDIES OF THE DATA

2.1. *A brief note about the use of distances*

Regarding the use of the inverse of the parallax as distance, there are numerous papers in which such equality is used for distances near the Sun (for example we can highlight: Vityazev & Tsvetkov (2009), Vityazev et al. (2011) (Makarov & Murphy. 2007) **which** applies to a subset of 42487 stars of Hipparcos fulfilling that $\pi/\sigma(\pi) > 5$ or Vityazev et al. (2017c)). On the other hand, in the 1997 version of Hipparcos, the uncertainties in the parallaxes were 1 mas,

Table 1. Initial statistics for 2MASS-Hip2 (* = stars with $r < 25pc$ are not considered; ** = we show data, in mas, for stars with $r \leq 600pc$)

Centered at $r =$	D_r	N	$\overline{r}$	$\overline{\Delta\alpha^*}$	$\overline{\Delta\delta}$	$\overline{\Delta\alpha^*_r}$	$\overline{\Delta\delta}_r$	$\sqrt{Pot}$
	S^2	58081	345.58	0.66	5.82	0.21	4.34	117.55
100	$[25, 200]^*$	24498	125.34	1.37	8.41	1.08	7.55	124.19
200	$[100, 300]$	30455	192.93	0.43	6.29	0.33	6.29	118.58
300	$[200, 400]$	23219	288.88	-0.09	5.34	-0.11	5.39	114.71
400	$[300, 500]$	16224	386.69	0.40	4.17	0.48	4.03	113.32
500	$[400, 600]$	10364	482.60	1.15	2.80	1.10	2.84	112.50

so Lutz-Kelker bias was not considered before 200 pc. However, given that there are new estimates for the stars of Hipparcos-2 from the publication of TGAS distances introduced in the paper Astraatmadja et al. (2016a) and the corresponding data (catalog available at http://www.mpia.de/homes/calj/tgas_distances/main.html), we have decided to make use of these new data.

However, in a preliminary study related to the use of the inverse of the trigonometric parallax as a biased approximation of the distance, we have created 1000 samples from the initial data, perturbing the AR and the DEC by a N(0,1) and the inverse of the parallax by 20% of its value times a N(0,1) We have verified that, considering all the samples, if we call m_i and M_i the minimum and maximum values, for the i-star, of the "distances" in Hipparcos-2 with the application of the disturbance, 90% of the stars that we have used verifies that $r_i < dG_i < M_i$, where dG_i are the distances provided in the file annexed to (Astraatmadja et al. 2016a), which could show a relatively high reliability in the results that will be obtained in our studies, in 3D, of the residuals for the stars of Hipparcos-2 compared with the corresponding positions in another catalog. In spite of this, given the aforementioned availability of distances for the stars of the TGAS, we have used them although the positions and proper motions are those corresponding to Hipparcos-2. With this choice, the reliability of our method and later results are based on a disturbance test with lower requirements, in which the RA and the DEC are still added a N (0,1) but to the distance, a 10% of itself times a N(0,1) is added. The results obtained are shown later in Table 5. Before that, we previously show in the following two subsections, the results of some elementary statistical studies about the qualitative and quantitative aspects of the data considered.

2.2. *Data quantitative aspects*

We initially consider the 66577 stars common to Hipparcos 2 (van Leeuwen 2007b) and 2MASS (Skrutskie et al, 2006) with known TGAS distances, we eliminate double stars, those with negative parallax, and considering that both residuals $\Delta\alpha^*, \Delta\delta$ are, in absolute value, minor than $200mas$. Under these conditions, we have the initial statistics seen in Table 1 (D_r indicates the domain to which the data in the corresponding line refer). We consider overlapping for a better follow-up of the continuity or discontinuity of the different quantities.

We calculated the mean of r ($\overline{r}$) for each slice, and the means in $\Delta\alpha^*, \Delta\delta$ in two different ways: the usual arithmetic mean and the weighted mean with the distance in pc: $\overline{\Delta\alpha^*}_r = \frac{\sum_{i=1}^N r_i \Delta\alpha_i^*}{\sum_{i=1}^N r_i}$, $\overline{\Delta\delta}_r = \frac{\sum_{i=1}^N r_i \Delta\delta_i}{\sum_{i=1}^N r_i}$. Finally, the square root of the power $\sqrt{\frac{[\Delta\alpha_i^*]^2 + [\Delta\delta_i]^2}{N}}$ is provided.

We can observe that the means in $\Delta\alpha^*, \Delta\delta$ are very similar, no matter if the weighting is the classical arithmetic or the one given by the distances. This may imply that the dependence $\Delta\alpha^*(r), \Delta\delta(r)$ (that can be seen, in a smooth way, in figure 3) is very accurate for the TGAS distances. The graphs of the density functions in $\Delta\alpha^*, \Delta\delta$ and r can be seen in Figures 1 and 2.

Another aspect to consider is the lack of normality of $\Delta\alpha^*, \Delta\delta$ (see, again, figure 1 for the 2MASS). This rather points to a "Gaussian Mixture" which confirms our interest to study different subsets of data, with respect to magnitudes or spectral types, for example. The dependence of r and also some physical properties, would indicate the search for clusters from a statistical point of view (not to be confused with star clusters). Finally, the distribution in r indicates that a large % of our star set have a radius $r \leq 600pc$ so we have selected the stars up to such a distance because our aim is devoted to the slices centered at the distances r=100, 200, 300, 400 y 500 pc. Employing these restrictions, only 58081 stars remain.

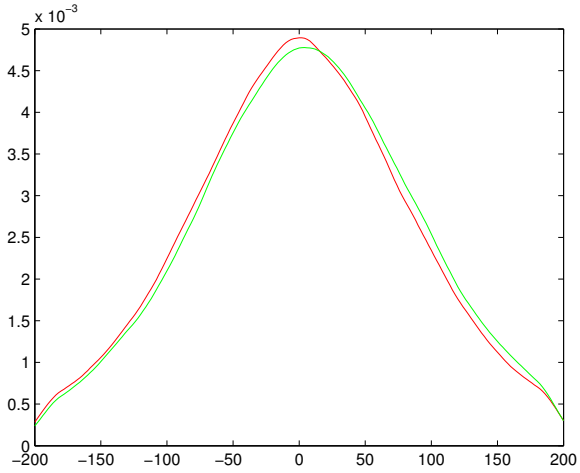

Figure 1. Density Functions for $\Delta\alpha^*$ (red),$\Delta\delta$ (green), in mas.

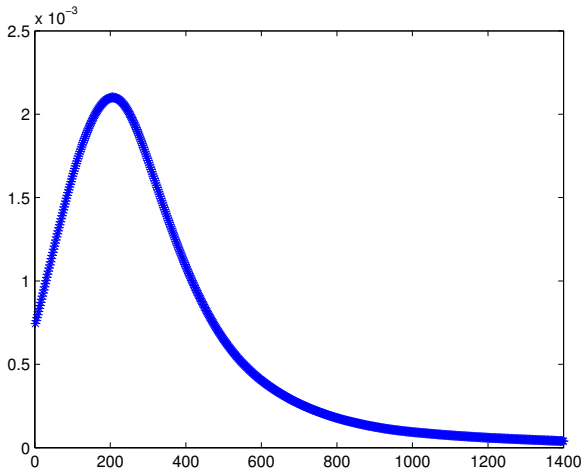

Figure 2. Distribution of r (in pc) for 2MASS.

2.3. *Data: qualitative aspects*

The magnitude is a property whose influence has been studied by (Bien et al. 1978) and (Schwann 2001) among others. In this section, we only give a brief description of the data that, in our case, take values between H_p-magnitudes -1.088 and 14.169. Figure 4 gives an idea of their probability density function (Hmag is taken from the Hipparcos2 catalog and here it is represented as H_p).

Artificially we have made a subdivision into $10m$ subintervals and have subsequently classified the stars according to $r-$slices of $200pc$. Approximately 75% of the stars are concentrated in the subsets that we have called m_5 and m_6, but other magnitudes have also been considered that also have good representativity in some of the selected $r-$intervals. More specifically, if $m_4 = [5.750, 7.153]\,, m_5 = [7.153, 8.556]$, $m_6 = [8.556, 9.959]$, $m_7 = [9.959, 11.363]$ and we consider the distances $[25, 600]$ pc .The numerical distribution can be seen in Table 2.

With respect to the spectral type, we have differentiated the two KM groups (K or M type) and the rest, obtaining 17243 for the first and 40838 for the second group, always with the general conditions indicated in the preceding subsection. Global distributions for KM and No-KM stars can be seen in Figure 5 and their statistics in Table 3, where we can see some information about the bias in the distributions of stars in KM and $No-KM$. Namely, the

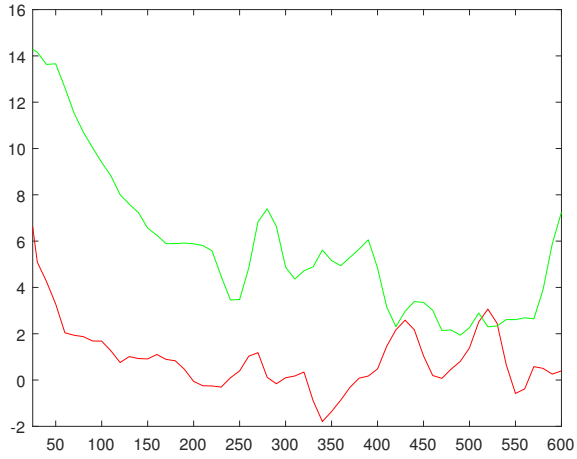

Figure 3. Graphic in smoothed means of $\Delta\alpha^*(r)$ (red),$\Delta\delta(r)$ (green), in mas.

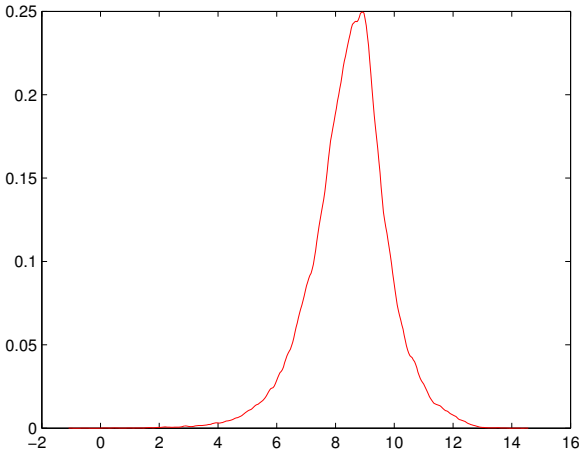

Figure 4. Density function for H_p-magnitude

Table 2. Numerical distribution regarding r and number of stars of the m_4, m_5, m_6, m_7 2MASS subsets.

Centered at $r =$	D_r	m_4	m_5	m_6	m_7
	S^2	4707	24888	28103	4263
100	$[25, 200]^*$	2947	9742	9968	1632
200	$[100, 300]$	2844	13048	12215	2254
300	$[200, 400]$	1331	10248	9867	1712
400	$[300, 500]$	624	6031	8558	952
500	$[400, 600]$	309	3588	5866	568

former subset has a greater bias in $\Delta\alpha^*$, while the latter subset has a greater bias in $\Delta\delta$. In table 4 we show the statistics for the spectral type in each of the magnitude subgroups.

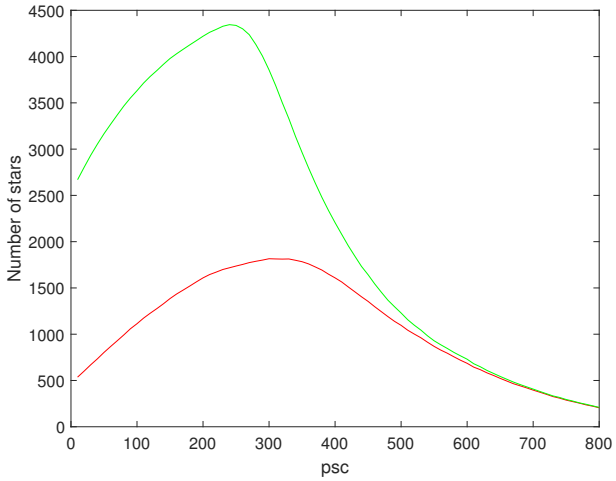

Figure 5. Star distribution for type K or M (KM) stars, in red, and the rest (No-KM), in green

Table 3. Numerical distribution (in mas) of stars of spectral type from K to M and the rest. Stars from $25pc$ to $99pc$ are included and also subdivision by intervals centered at r from $100pc$ to $800pc$. 2MASS-Hip2. r is the value in pc where the slice is centered

Spectral	$r =$	D_r	N	$\overline{\Delta\alpha^*}$	$\overline{\Delta\delta}$	$\sigma_{\Delta\alpha^*}$	$\sigma_{\Delta\delta}$	$\overline{\Delta\alpha^*_r}$	$\overline{\Delta\delta}_r$	$\sqrt{Pot}$
		S^2	40838	-0.73	7.26	82.32	80.88	-1.78	5.91	115.6
No KM	100	$[25, 200]$	21360	0.50	8.66	88.29	84.52	0.21	7.97	122.6
	200	$[100, 300]$	24286	-0.41	6.87	83.24	81.25	-0.54	6.65	116.5
	300	$[200, 400]$	14740	-1.17	5.81	77.56	78.01	-1.25	5.85	110.2
	400	$[300, 500]$	8465	-2.03	5.09	75.18	76.24	-2.08	4.50	107.2
	500	$[400, 600]$	4738	-3.38	4.94	72.84	75.17	-3.52	5.01	104.8
		S^2	17243	4.01	3.45	86.62	87.15	4.03	1.87	123.0
KM	100	$[25, 200]$	3138	7.31	6.65	97.68	92.57	7.18	4.56	134.9
	200	$[100, 300]$	6169	3.77	3.99	89.94	88.71	3.21	3.98	126.4
	300	$[200, 400]$	8479	1.79	4.53	86.03	86.65	1.73	4.65	122.2
	400	$[300, 500]$	7759	3.06	3.15	83.64	85.41	3.21	3.00	119.6
	500	$[400, 600]$	5626	4.96	1.0	82.27	85.24	4.94	1.05	118.6

Table 4. Numerical distribution (in mas) of 2MASS-Hip2 stars of spectal type from K to M and the rest. Subdivision by magnitudes are included considering only our m_4, m_5, m_6 and m_7 subsets.

Spec/Mag	N	$\overline{\Delta\alpha^*}$	$\overline{\Delta\delta}$	$\sigma_{\Delta\alpha^*}$	$\sigma_{\Delta\delta}$	$\overline{\Delta\alpha^*_r}$	$\overline{\Delta\delta}_r$
No KM							
& m_4	3185	-1.55	4.61	86.11	86.45	-4.00	4.69
& m_5	15392	-0.72	6.50	83.96	83.50	-3.24	4.80
& m_6	18765	-0.64	6.62	80.77	79.47	-2.06	5.65
& m_7	3329	-3.74	13.90	73.26	66.89	-4.58	11.07
KM							
& m_4	1402	15.95	2.20	95.91	96.39	19.34	4.75
& m_5	8186	4.80	2.94	88.38	90.17	7.40	1.69
& m_6	6936	2.46	3.48	81.71	82.54	2.56	2.28
& m_7	583	-4.33	6.63	90.22	87.09	-2.74	-0.81

3. THE METHODS

In this section we present a brief justification of why we use other than the current procedures to deal with the problem. Next, we will introduce the formulations that allow to deal with the problem from a continuous point of view.

3.1. *Continuous vs. discrete problem*

The problem about the three-dimensional study of the differences has recently been partially addressed by Vityazev (Vityazev & Tsvetkov 2013) to the residuals of Hipparcos2 and UCAC4. Such work has taken into account the discrete set of data, the adjustment model and the statistical method for the allocation of formal errors and, if appropriate, the acceptance or denial of a determined computed value for some parameter (contrast of hypotheses).

However, it is possible to go back to the work of Mignard & Morando (1990) to see the use of VSH in catalog problems. From then, two issues regarding catalogs have been studied: the one concerning the position and that of the kinematical study of the galaxy from the proper motions. About the former we can highlight its application to Hipparcos-FK5 (Mignard & Klioner 2012) and (Marco et al. 2004), or to those made by Vityazev et al. for the UCAC4-PPMXL (Vityazev & Tsvetkov 2015), XPM-UCAC4 (Vityazev et al. 2017a), among others. Regarding the application in kinematic studies, we can mention those obtained by Vityazev et al. (Vityazev & Tsvetkov (2009) with Hipparcos and a catalog test between 200 and 300pc, Vityazev et al. (2011) for Tycho-2, Vityazev & Tsvetkov (2013) for UCAC4, Vityazev & Tsvetkov (2014) for UCAC4, PPMXL and XPM, Vityazev & Tsvetkov (2017b) for Tycho-2 using TGAS, (Vityazev et al. 2017c) for UCAC4, PPMXL, TGAS, using RAVE5 and the use of VSH in Marco et al. (2015) applied to the proper motions of Hipparcos2 and introducing non-parametric methods of adjustment. We can also reference the study conducted by Mignard (2000) that, although it does not use VSH, does make an interesting distinction between spectral types for the results of OMM model of the Hipparcos kinematics.

As we have already mentioned in previous articles (Marco et al. 2004), (Marco et al. 2015), the choice of model requires assuming that the function to be adjusted belongs to a certain space of functions and then the least squares integral condition is applied, which allows the calculation of the parameters. The fact of working with a discrete set of data makes that such calculations to be, actually, estimates. In this sense, most authors prefer to make discrete least squares adjustments (which we will call DLS). Accepting, of course, that this procedure provides the coefficients for the least-variance unbiased estimator (in the discrete sense), there are some facts that make us think of a variation of the procedure. First, the original data are not necessary unbiased (and this is why the estimator obtained - the model with the corresponding coefficients - will not be the unbiased minimum variance estimator). Second, let us remember that the data are being adjusted to a continuous function and the model is nothing more than the truncated development, up to the desired order, of an infinite series. Such series development can be assumed to exist for a function with square integrable in the working domain (for example, in the sphere). The fact of working with the DLS method implies that no use is made of the analytical properties in which the continuous problem is formulated and a good part of the power of the theoretical procedure may be lost. We then go on to describe the continuous extent of the problem.

Suppose that we want to determine a function $f(x)$ belonging to a Hilbert space H, with $x \in D$, the work domain, and that function verifies the necessary hypotheses that assure the existence of a convergent series development (not punctual convergence, but convergence in the norm of the functional space). Suppose we work with an orthogonal basis $(\phi_i)_{i\geq 0}$. Then, the completeness property tells us that there exist (unique) coefficients α_i such that:

$$f(x) = \sum_{i\geq 0} \alpha_i \phi_i(x) \tag{1}$$

Remember that this equality is, in fact, symbolic. What it really means is that:

$$\lim_{n\to\infty} \left\| f - \sum_{i=0}^{n} \alpha_i \phi_i \right\|_H \tag{2}$$

where $\| \ \|_H$ represents the norm associated to the inner product in H denoted by $\langle , \rangle_H$. Thanks to the orthogonality and completeness properties of the basis we can assure that:

$$\alpha_k = \frac{\langle f, \phi_k \rangle_H}{\langle \phi_k, \phi_k \rangle_H} \ \forall k \geq 0 \tag{3}$$

The importance of this formula is that each coefficient is found independently of the others. Note that this does not happen with a discrete treatment of the problem because in this case, we have to choose an "a priori" order for the development and if we decide to increase that order, the coefficients must be recalculated again. This is a huge drawback. The reason is that the functional orthogonality of the basis enables the previous formula to be exact for each index. In the discrete case, with the DLS method, the theoretical functional orthogonality does not become algebraic orthogonality of the normal matrix that estimates the coefficients. This is why recalculation is mandatory if the order of development is changed. On the contrary, a discrete formulation in which we select a mesh in the domain D with equispaced points (in each dimension of D), retains the theoretical functional orthogonality to that discrete step. You would get approximate values:

$$\widehat{\alpha}_k = \frac{\left\langle \widehat{f}, \phi_k \right\rangle_{H_m}}{\langle \phi_k, \phi_k \rangle_{H_m}} \ \forall \ k \geq 0 \tag{4}$$

where $\widehat{f}, \widehat{a}_k$ are approximations obtained by working in the discrete space H_m, m representing the discrete meshing and $\langle , \rangle_{H_m}$ the discretization of the inner product in H. No recomputation of the coefficients is required if the order is increased.

In our case, the Hilbert space will be that of functions (or vector fields) of square integrable in the sphere: $L^2(S^2)$, and the v product will be the integral over the sphere. Note that the calculation of the estimates of $\widehat{\alpha}_k$ will be performed by applying a numerical integration. To complete the procedure, we only need to see how to determine $\widehat{f}$. Let us recall that we initially start from a set of discrete data $\alpha_i, \delta_i, r_i, \Delta\alpha_i^*, \Delta\delta_i$ and we can assume that they are realizations of random discrete or continuous variables . We work on the second assumption and we will use non-parametric kernel estimation, and kernel local polynomial linear regression that is useful for working with vector fields.

3.2. *Kernel Estimations*

In this subsection we provide the exposition of the procedures for determining density functions, unidimensional regressions to fit the function, and multidimensional local polynomial formulation (which adjusts the function and the partial derivatives up to a predetermined order, which for us will be only one). During the brief presentation, the necessary references will be cited for an extension of the concepts, including theoretical results as well as their practical application.

3.2.a) A kernel K is a non-negative function, defined in a domain D and such that $\int_D K(x)dx = 1$, $\int_D xK(x)dx = 0$ and $\int_D x^2K(x)dx < +\infty$. Simple and usual examples are Epanechnikov kernel: $K(x) = 1_{|x|\leq 1}\frac{3}{4}(1-x^2)$ or Gauss kernel $K(x) = \frac{1}{2\pi}\int_{-\infty}^{x}\exp(-t^2)dt$. Its properties, in terms of statistical efficiency, can be found in (Simonoff 1996), (Fan & Gijbels 1996) or (Wand & Jones 1995). The density function $f(x)$ of a random variable (r.v.) X is estimated by:

$$\widehat{f}(x) = \frac{1}{Nh}\sum_{k=1}^{N} K(\frac{x-x_k}{h_x}) \tag{5}$$

where (x_k) are the discrete data of the r.v. and h_x is the so-called bandwidth which can be constant or variable and in which the sub-index refers to the r.v. The higher value of h_x the smoother the estimator and the lesser value of h_x the lesser smooth estimator. The optimization of this parameter is done minimizing the AMISE (Asymptotic Mean Integral Squared Estimation), whose value for this one-dimensional problem is $h_{opt} = N\widehat{\sigma}^{-0.2}$ with N the size of the sample and $\widehat{\sigma}$ the standard deviation of the data. This topic and the extension to the multidimensional case is immediate and can be seen in the previous references. The optimal values of the bandwidth are obtained in the case of a dimension d, as $H = \left(\frac{4}{d+2}\right)^{\frac{1}{d+4}} diag\left(\Sigma^{\frac{-1}{2}}\right) n^{\frac{-1}{d+4}}$ (Simonoff 1996), with H the vector of the different values of h and Σ the variance-covariance matrix.

3.2.b) Let us now consider the case of an r.v. (X, Y) with discrete data (x_k, y_k). Let $\widehat{f}_{X,Y}(x, y)$ denote the kernel estimate of the joint density function. If we assume that the r.v. Y depends on the r.v. X, the regression of Y on X will be $y = m(x)$. The precise definition is $y = m(x) = E[Y|\, X = x] = \int y f_{Y|X=x}(y|\, X = x)dy$, where $f_{Y|X=x}$ is the conditional probability which, by the Total Probability Theorem, verifies that $f_{X,Y}(x, y) = f_{Y|X=x}(Y|\, X = x)f_X(x)$ (hereafter, we will omit references in densities to r.v.s, except where the context requires otherwise). A substitution in the exact formula of the regression, but applying the kernel approximations of the densities (since they are unknown),

provides an estimate of the regression, known as Nadaraya-Watson (since there is no danger of confusion we use h instead of h_x):

$$y = \widehat{m}(x) = \sum_{k=1}^{N} \omega_k y_k \quad , \quad \omega_k = \frac{K(\frac{x-x_k}{h})}{\sum_{j=1}^{N} K(\frac{x-x_j}{h})} \tag{6}$$

It is interesting to remark that the Nadaraya-Watson method has the following characteristic: if Y is an r.v. dependent on another r.v. X, the estimation at a point x is the value $\widehat{\beta}(x)$ that minimizes (in β) the expression:

$$\frac{1}{Nh} \sum_{i=1}^{n} (Y_j - \beta)^2 K\left(\frac{x - x_j}{h}\right) \tag{7}$$

which is nothing more than the discretization (from integral to summation) of the variance of $Y|_{X=x}$ with the approximate density of the kernel and with the solution $\widehat{\beta} = E\left[Y|_{X=x}\right]$. In this sense, the Nadaraya-Watson formula is easily generalizable to the case of an r.v. Y (with $Y = \Delta\alpha^*$ or $\Delta\delta$) depending on (α, δ, r):

$$y = \sum_{k=1}^{N} \omega_k y_k \quad , \quad \omega_k = \frac{K(\frac{\alpha-\alpha_k}{h_\alpha}) K(\frac{\sin\delta - \sin\delta_k}{h_{\sin\delta}}) K(\frac{r-r_k}{h_r})}{\sum_{j=1}^{N} K(\frac{x-x_j}{h_\alpha}) K(\frac{\sin\delta - \sin\delta_j}{h_{\sin\delta}}) K(\frac{r-r_j}{h_r})} \tag{8}$$

Where we have worked with $\sin\delta$ and not with δ.

3.2.c) The regressions given in the two previous subsections refer to scalar functions. However, our work is based on vector fields in space, that will be three-dimensional or two-dimensional, depending on wether we work in $\mathbb{R}^3$ or, for each fixed r, in S^2 either in Cartesian coordinates or in spherical coordinates. In the latter case, if $\mathbf{X}$ is the position vector of a point, in the sphere of radius r, then small variations in α and δ will also induce a change in the position vector and, thus, the residual vector field is:

$$\Delta\mathbf{X} \equiv \mathbf{V}(\alpha, \delta) = V^\alpha(\alpha, \delta)\mathbf{e}_\alpha + V^\delta(\alpha, \delta)\mathbf{e}_\delta = (\Delta\alpha^*)\,\mathbf{e}_\alpha + (\Delta\delta)\,\mathbf{e}_\delta \tag{9}$$

We have denoted as $V^\alpha(\alpha, \delta) = \Delta\alpha^*, V^\delta(\alpha, \delta) = \Delta\delta$ the scalar fields of residuals and, as usual, by $\mathbf{e}_\alpha, \mathbf{e}_\delta$ the unit vectors in the tangent plane, at the considered point, and in the respective directions given by the right ascension and the declination. In Cartesian coordinates, these vectors are:

$$\mathbf{e}_\alpha = \frac{1}{\cos\delta}\frac{\partial\mathbf{X}}{\partial\alpha} = \begin{bmatrix} -\sin\alpha \\ \cos\alpha \\ 0 \end{bmatrix}, \mathbf{e}_\delta = \frac{\partial\mathbf{X}}{\partial\delta} = \mathbf{X} \times \mathbf{e}_\alpha = \begin{bmatrix} -\cos\alpha\sin\delta \\ -\sin\alpha\sin\delta \\ \cos\delta \end{bmatrix} \tag{10}$$

As already mentioned in section 1, the consideration of the three-dimensional problem provides residuals $\Delta\alpha^* = \Delta\alpha^*(r, \alpha, \delta), \Delta\delta = \Delta\delta(r, \alpha, \delta)$ where the dependence of r makes it possible to choose two ways of working: a) fixing certain values of r (the slices mentioned in section 1) and then take $\Delta\alpha^* = \Delta\alpha^*(\alpha, \delta), \Delta\delta = \Delta\delta(\alpha, \delta)$ for each of those r; b) work directly in 3 dimensions, in any coordinate system. As we will see later, the work in Cartesian coordinates has, in some cases, advantages when dealing with points near the poles. By now, we will limit ourselves to describing the approach to arrive at a generic exposition of the local polynomial regression method (first degree) to be used with the vector field component functions. For convenience, it will be exposed for two variables, although its generalization to the case of three or more variables is immediate.

The kernel polynomial local regression provides estimates of the function and its derivatives up to a predetermined order. Again, for simplicity, we will limit ourselves to the case where only derivatives of first order are required, that is, a local linear polynomial regression. To see how this problem is addressed, let us consider that we are looking for a fit between random variables such as $Y_i = m(\mathbf{X}_i)$, where $\mathbf{X}_i$ is a random vector of dimension 2 and we assume that:

$$m(\mathbf{X}_i) \simeq m(\mathbf{x}) + (D^1 m)_{\mathbf{x}}(\mathbf{X}_i - \mathbf{x}) \tag{11}$$

as linear approximation. We search the estimator $\left\{\widehat{m}(\mathbf{x}), \widehat{\frac{\partial m}{\partial x_1}}(\mathbf{x}), \widehat{\frac{\partial m}{\partial x_2}}(\mathbf{x})\right\} \equiv \{\widehat{m}(\mathbf{x}), \widehat{m_{11}}(\mathbf{x}), \widehat{m_{12}}(\mathbf{x})\}$ where the second notation is for convenience and if, for example, the r.v. is $\Delta\alpha^*$, $\widehat{m}$ indicates the estimation of the function, while $\widehat{m_{11}}, \widehat{m_{12}}$ indicate the estimates of the partial derivatives of the random vector with respect to α, δ respectively. Since

m is a scalar function, the first subscript in both expressions of $\widehat{m_{11}}, \widehat{m_{12}}$ is not necessary here, but they are shown since for the case where m had several components, they should all be considered. The estimates $\{\widehat{m}(\mathbf{x}), \widehat{m_{11}}(\mathbf{x}), \widehat{m_{12}}(\mathbf{x})\}$ are the solution to the problem:

$$\begin{aligned} &\left\{\widehat{b_0}(\mathbf{x}), \widehat{b_{11}}(\mathbf{x}), \widehat{b_{12}}(\mathbf{x})\right\} = \\ &= \min_{\left\{\widehat{b_k}(\mathbf{x})\right\}} \left\{Y_i - b_0(\mathbf{x}) - b_{11}(\mathbf{x})(X_{i,1} - x_1) - b_{12}(x)(X_{i,2} - x_2)\right\}^2 K_{\mathbf{h},i\mathbf{x}} \end{aligned} \tag{12}$$

being $\mathbf{x} = (x_1, x_2)^t, \mathbf{h} = (h_1, h_2)^t$ and $K_{\mathbf{h},i\mathbf{x}}$:

$$K_{\mathbf{h},i\mathbf{x}} = \frac{1}{h_1} K(\frac{X_{i,1} - x_1}{h_1}) \frac{1}{h_2} K(\frac{X_{i,2} - x_2}{h_2}) \tag{13}$$

For the explicit formulas to program the computation of the estimators, see Masry & Fan (1997).

4. MODELS OF ADJUSTMENTS

In this section, we present two different models of adjustment, with two different objectives: the first one refers to the global study of the vector fields of the residuals and the second sets the stage for a local study of such residuals. More specifically, the first model is a global adjustment development in VSH, already mentioned in previous sections. Given the lack of known significance for the coefficients of the developments, beyond the coefficients of the toroidal harmonics of order one representing the rotation between both catalogs, we limit ourselves to developments of first order. Already in section 5, in its practical application, we will see that depending on whether one field or another is considered in terms of spectral types, magnitudes and distances, such coefficients differ from one development to other. Thus, we will show the dependence of the systematisms, using the vector fields, of the different physical magnitudes considered. As for the second decomposition used, this consists in the application of the Helmholtz Theorem that enables to split a vector field into its rotational and irrotational components. This latter component is the gradient of a scalar field that, moreover, we can obtain as a development in surface spherical harmonics (in the present work, we have experimentally verified that a development of 5th order contains practically the complete information of the irrotational part of each considered vector field). Obtaining such potential is evident and the procedure is explained in section 5.2. We are interested in areas of the sphere where the irrotational component of the field is dominant. In these cases, the relative extremes of the potential function (local maxima and minima) are very close to critical points of the working vector field (sources and shrinks, respectively). So we are using this development to carry out a local study of the residuals. It is important to highlight that the local properties of the different fields that are associated to certain physical properties (spectral type, magnitude, as well as distance), that is, the patterns that we obtain, do not appear in the global field in which only the distance (or not even that, as in the case of a 2D vector field) is considered. Finally, in a later section, we will see a possible justification, which remains only as a hypothesis, for the emergence of the critical points, outlining a possible way to advance further in this local study.

4.a) At this point, we assume that after the application of the statistical procedures of the previous section, we have carried out the studies on the r.v. and estimates of the components of the vector field $\mathbf{\Delta X}$ have been found. This field is a simplified version of another three-dimensional field $\mathbf{F}$ that depends on the variables r, α, δ which we assume to verify the necessary conditions to be developed in Vector Spherical Harmonics (VSH henceforth. For convergence results see Jeffreys (1967))

$$\mathbf{F}(r, \alpha, \delta) = \sum_{n, |m| \leq n} [r_{nm}\mathbf{R}_{nm} + s_{nm}\mathbf{S}_{nm} + t_{nm}\mathbf{T}_{nm}] \tag{14}$$

where $\mathbf{R}_{nm}, \mathbf{S}_{nm}, \mathbf{T}_{nm}$ are the vectors (orthogonal and complete system of the functions with integrable square in the sphere of radius r) whose coefficients represent the radial, spheroidal and toroidal parts, respectively of the field F. These vectors are given by the expressions:

$$\mathbf{R}_{nm} = Y_{nm}\mathbf{r}, \mathbf{S}_{nm} = r\nabla Y_{nm}, \mathbf{T}_{nm} = -\mathbf{r} \times \nabla Y_{nm} \tag{15}$$

where $\mathbf{r}$ is the position vector, r its modulus and Y_{nm} are the ordinary surface spherical harmonics (see Annexes A and B). By the orthogonality, the different coefficients are calculated independently by the formula given above (3)

and (4). Estimates of the coefficients are performed by a polynomial linear local regression of the components of the field $\mathbf{\Delta X} = (\Delta\alpha^*)\,\mathbf{e}_\alpha + (\Delta\delta)\,\mathbf{e}_\delta$, in a grid of equispaced points over each sphere with a preset radius r.

4.b) The decomposition used in the preceding section is of first order and allows obtaining the coefficients $s_{1,0}, s_{1,1}, s_{1,-1}$ and $t_{1,0}, t_{1,1}, t_{1,-1}$. These last ones represent the rotation between both catalogs, deduced from the vector field of the residuals, but the $s_{1,0}, s_{1,1}, s_{1,-1}$ values (unlike those that are obtained in the vector field of the proper motions of the considered catalog, applied to stellar kinematics) do not have a clear physical meaning. Even so we propose an indirect approach based on the Helmholtz decomposition theorem. This result states that a vector field, under certain assumptions of regularity that we will assume, can be decomposed into its rotational part (solenoidal or divergence-free) and in its non-rotational part, which comes from a scalar potential. Since, for a given r_0, we are working on a sphere, we can apply to such a potential a spherical surface harmonic development of the desired order. Thanks to the properties of the spherical harmonics as eigenfunctions of the Laplace-Beltrami operator, it is possible to determine the coefficients of the potential by considering the divergence of the field. More specifically, let ϕ be a potential such that given a vector field $\overrightarrow{X}$ in the sphere, Helmholtz theorem states that there exists a (unique) decomposition in the form:

$$\overrightarrow{X} = \overrightarrow{\nabla\phi} + \overrightarrow{\nabla} \times \overrightarrow{u} \tag{16}$$

where the potential gradient ϕ, $\overrightarrow{\nabla\phi}$ is rotational-free, the rotational $\overrightarrow{\nabla} \times \overrightarrow{u}$ is divergence-free.

The calculation process is as follows:

4b-1) We find the divergence of the field, which provides the laplacian of the potential ϕ:

$$div\overrightarrow{X} = \Delta\phi \tag{17}$$

4b-2) We find ϕ and we suppose it developed in surface spherical harmonics:

$$\phi(\alpha, \delta) = \sum_{n,m} \alpha_{nm} Y_{nm}(\alpha, \delta) \tag{18}$$

If we apply the property that the harmonics are eigenfunctions of the Laplace-Beltrami operator, then we have:

$$\Delta\phi = \sum_{n,m} \alpha_{nm} \Delta Y_{nm} = \sum_{n,m} \left[-n(n+1)\alpha_{nm}\right] Y_{nm} \tag{19}$$

4b-3) The usual inner product in the Hilbert space $L^2(S^2)$ allows to obtain the components α_{nm}

$$\alpha_{nm} = -\frac{1}{n(n+1)} \frac{\langle \Delta\phi, Y_{nm} \rangle}{\langle Y_{nm}, Y_{nm} \rangle} \tag{20}$$

5. RESULTS

We divide this section into two subsections showing the coefficients of the VSH of the 2MASS-Hip2 vector field. Then, we perform a comparison between the potentials and vector fields for each slice for 2MASS-Hip2. And finally, we relate empirically the critical points with the same points on the surface of the V_T-magnitude for Tycho-2.

5.1. *Coefficients of the vector fields*

Before performing the calculations for the available data and in order to carry out a test on the reliability of the results that are given throughout the section, we generated 1000 samples for the 2MASS catalog, perturbing the residuals in right ascension and declination using a N(0, 1), and the distance with 10% of its value multiplied by a N(0,1). The results for the larger slices (those centered from $r = 100$ pc to $r = 500$ pc) are shown in table 5, including the actual values obtained for all the original non-perturbed data. After this, we compute the developments in VSH for all the KM / No-KM, m_4 to m_7 classifications and the mixtures between them, tapping different overlapping slices centered on $r = 100, 200, 300, 400, 500$ all in pc. We can observe that all the factors r, m, spectral type, have influence on them. In the first place, m_4 and KM-m_4 highlight the value of $t_{1,0}$. Regarding m_5 and No-KM-m_5, the highest values are reached in $s_{1,0}$. For m_6 the same coefficient ($s_{1,0}$) stands out correlated with both, KM and No-KM. Unfortunately, for m_7 no results can be shown in the case of KM- m_7 for any value of r or in the case of No-KM- m_7 for $r = 400$ pc or $r = 500$ pc, due to the low number of stars) So practically the maximum size in all the magnitudes falls on the same coefficient, different for each catalog, and with the same correlations with KM, No-KM or both. The exception is in m_4 with $t_{1,0}$ and its correlation KM-m_4.

Table 5. First Order VSH, up to 500*pc*. 2MASS-Hip2. r means the center of the slice. We also show the sample results and errors for the main slices.

$r=$	N	$s_{1,0}$	$s_{1,1}$	$s_{1,-1}$	$t_{1,0}$	$t_{1,1}$	$t_{1,-1}$
100	24498	9.70 ± 0.08	3.25 ± 0.09	0.67 ± 0.09	2.87 ± 0.08	1.55 ± 0.09	3.57 ± 0.09
		9.81	3.19	0.73	2.85	1.58	3.43
200	30455	8.26 ± 0.07	3.55 ± 0.07	0.45 ± 0.07	2.25 ± 0.07	1.40 ± 0.07	3.96 ± 0.08
		8.28	3.63	0.45	2.24	1.41	3.97
300	23219	6.64 ± 0.11	3.56 ± 0.10	0.56 ± 0.10	1.98 ± 0.10	0.98 ± 0.10	4.44 ± 0.10
		6.68	3.60	0.57	1.98	0.99	4.50
400	16224	5.45 ± 0.16	3.38 ± 0.15	1.02 ± 0.15	2.21 ± 0.16	-0.20 ± 0.16	4.50 ± 0.16
		5.47	3.38	1.01	2.25	0.28	4.58
500	10364	4.12 ± 0.25	3.40 ± 0.23	1.13 ± 0.24	2.73 ± 0.24	-1.13 ± 0.24	4.15 ± 0.23
		4.11	3.38	1.17	2.83	1.23	4.14
S^2	58081	7.33	3.43	0.80	2.12	0.81	3.81
S^2(with weights)		7.39	3.44	0.69	2.38	0.84	3.65

Table 6. VSH coefficients for m_4 magnitudes 2MASS-Hip2. r means the center of the slice

$r=$	N	$s_{1,0}$	$s_{1,1}$	$s_{1,-1}$	$t_{1,0}$	$t_{1,1}$	$t_{1,-1}$
100	2947	5.87	3.84	2.60	4.44	1.13	2.51
200	2844	4.39	4.79	0.39	6.76	1.50	3.66
300	1331	2.62	7.04	-4.09	10.98	2.55	4.52
S^2/m_4	4587	5.62	4.19	-0.05	6.64	0.69	2.62

Table 7. VSH coefficients for m_5 magnitudes. 2MASS-Hip2. r means the center of the slice

$r=$	N	$s_{1,0}$	$s_{1,1}$	$s_{1,-1}$	$t_{1,0}$	$t_{1,1}$	$t_{1,-1}$
100	9742	9.44	4.58	1.75	3.00	1.51	3.42
200	13048	8.41	4.39	1.44	2.22	1.57	3.58
300	10248	7.02	3.42	1.36	1.77	1.04	4.03
400	6031	5.41	2.09	1.49	3.26	-0.29	5.15
500	3588	2.25	1.64	0.15	5.76	-2.08	5.33
S^2/m_5	23568	7.43	2.49	1.40	3.07	0.82	3.24

Regarding the toroidal components, we have already highlighted the size of $t_{1,0}$ for m_4. For m_5 and m_6 we can highlight a change of sign in $t_{1,1}$ in r = 400 pc and r = 500 pc that is only observed, very slightly, in KM-m_5 and No-KM-m_5, respectively.

The next variation in sign is given in $t_{1,0}$ and $t_{1,1}$ for m_7 in r= 300 pc. Both coefficients in No-KM-m_7 are negatives for all value of r where the calculations are significant (note that in the subgroup KM-m_7 there are very few stars per slice and no conclusions can be drawn). It should be noted that, in general, there are trends in the increase or decrease of the values of many parameters when increasing r. It seems clear that these trends do not have a random origin and point, once more, to the influence of distance on the values of the coefficients. All the details can be seen in tables from 6 to 19.

5.2. *Comparison between potentials, vector fields on the slices of 2MASS and V_T Tycho-2 surfaces*

A visual inspection of the 2MASS-Hipparcos2 residual vector fields reveals a great mix of properties in terms of their singular points. Recall that after the formula (16) the non-rotational part of the field comes from a potential, for each

Table 8. VSH coefficients for m_6 magnitudes. 2MASS-Hip2. r means the center of the slice

$r=$	N	$s_{1,0}$	$s_{1,1}$	$s_{1,-1}$	$t_{1,0}$	$t_{1,1}$	$t_{1,-1}$
100	9968	10.21	2.18	0.98	2.50	1.78	3.97
200	12215	8.19	2.93	0.78	1.57	1.68	4.36
300	9867	6.06	3.52	0.19	1.20	0.92	4.85
400	8558	4.98	3.99	1.46	1.08	-0.35	4.42
500	5866	4.46	4.09	1.86	1.54	-1.17	3.50
S^2/m_6	28701	7.50	3.23	0.28	1.12	0.77	3.70

Table 9. VSH coefficients for m_7 magnitudes. 2MASS-Hip2. r means the center of the slice

$r=$	N	$s_{1,0}$	$s_{1,1}$	$s_{1,-1}$	$t_{1,0}$	$t_{1,1}$	$t_{1,-1}$
100	1632	17.83	2.63	3.17	4.29	2.69	1.08
200	2254	14.97	0.14	0.81	5.07	2.81	0.77
300	1712	13.42	1.05	2.66	-5.94	-2.50	1.54
S^2/m_7	3912	14.88	1.22	1.60	5.18	1.39	2.45

Table 10. VSH coefficients for No-KM magnitudes. 2MASS-Hip2. r means the center of the slice

$r=$	N	$s_{1,0}$	$s_{1,1}$	$s_{1,-1}$	$t_{1,0}$	$t_{1,1}$	$t_{1,-1}$
100	21360	10.12	3.69	1.27	2.05	1.27	3.46
200	24286	8.96	3.80	0.70	1.51	1.20	3.91
300	14740	7.36	3.94	0.57	1.01	0.54	4.74
400	8465	6.30	3.89	1.45	0.84	-1.66	5.20
500	4738	6.18	3.53	2.60	0.72	-3.73	5.46
$S^2/No-KM$	40808	9.24	3.28	1.14	1.53	0.44	4.20

Table 11. VSH coefficients for KM magnitudes. 2MASS-Hip2. r means the center of the slice

$r=$	N	$s_{1,0}$	$s_{1,1}$	$s_{1,-1}$	$t_{1,0}$	$t_{1,1}$	$t_{1,-1}$
100	3138	8.16	1.13	-2.34	7.04	3.34	2.68
200	6169	6.54	2.37	-3.27	4.33	2.74	3.33
300	8479	5.73	2.07	0.86	3.08	2.21	3.08
400	7759	4.65	1.86	0.79	3.42	1.38	2.93
500	5626	2.34	2.49	0.05	4.37	0.74	2.11
S^2/KM	17243	4.95	1.82	-0.05	4.58	1.77	2.47

r, found with (18) and (20) up to fifth order (already fulfilling formula (17)). We show in Figure 6 the contour lines corresponding to the potential of the $[25, 200]$ pc slice.

Tables 20 to 24 show some additional information with the singular points of the potential for each r and the critical points of the vector fields. We denote as area $I = \{\alpha \geq \pi, \delta < 0\}$, area $II = \{\alpha \geq \pi, \delta \geq 0\}$, area $III = \{\alpha < \pi, \delta \geq 0\}$, area $IV = \{\alpha < \pi, \delta < 0\}$

We are going to show some examples in which it is appreciated that a maximum of this potential corresponds to a source of the vector field, and a minimum of the potential corresponds to a shrink of the vector field. We recall that the singular points and their situation regarding the critical points of the potential can be seen in tables 20 to 24. Given that there are many graphs, we have considered adequate to only show some of the most relevant in figures 7

Table 12. VSH coefficients for $No-KM$ spectral types and m_4 magnitudes. 2MASS-Hip2. r means the center of the slice. The entries correspondig to r=500 are not included because there are only 191 stars.

$r=$	N	$s_{1,0}$	$s_{1,1}$	$s_{1,-1}$	$t_{1,0}$	$t_{1,1}$	$t_{1,-1}$
100	2281	6.18	5.04	5.24	1.32	0.99	4.33
200	1834	5.13	4.87	2.23	0.96	0.31	4.62
300	713	2.25	7.65	-1.18	1.51	2.24	8.17
400	335	2.23	11.78	-5.64	2.24	3.52	10.83
$S^2/No-KM-m_4$	3185	6.51	4.21	3.44	1.58	0.65	4.85

Table 13. VSH coefficients for $No-KM$ and m_5 magnitudes. 2MASS-Hip2. r means the center of the slice

$r=$	N	$s_{1,0}$	$s_{1,1}$	$s_{1,-1}$	$t_{1,0}$	$t_{1,1}$	$t_{1,-1}$
100	8563	10.21	4.80	2.23	2.93	1.58	3.41
200	9196	9.04	4.34	1.42	1.78	1.72	3.03
300	5504	7.55	5.21	0.54	1.80	1.88	4.18
400	2716	5.30	4.50	1.79	2.82	0.66	5.91
500	1325	2.13	2.14	1.39	3.45	-0.09	8.46
$S^2/No-KM-m_5$	15392	9.35	3.41	1.73	2.88	1.73	3.90

Table 14. VSH coefficients for spectral types spectral $No-KM$ and m_6 magnitudes . 2MASS-Hip2. r means the center of the slice

$r=$	N	$s_{1,0}$	$s_{1,1}$	$s_{1,-1}$	$t_{1,0}$	$t_{1,1}$	$t_{1,-1}$
100	9199	10.12	3.15	-0.78	1.78	1.30	3.57
200	11016	8.45	3.57	-0.39	0.91	1.12	4.10
300	6834	6.08	3.76	-0.19	1.28	0.35	5.53
400	4477	5.16	4.06	1.50	0.98	-2.36	5.81
500	2732	5.69	4.34	2.45	1.80	-5.22	5.28
$S^2/No-KM-m_6$	18765	8.21	3.11	0.28	0.87	0.05	4.54

Table 15. VSH coefficients for spectral types $No-KM$ and m_7 magnitudes. 2MASS-Hip2. r means the center of the slice. The entries correspondig to r=500 are not included because there are only 461 stars.

$r=$	N	$s_{1,0}$	$s_{1,1}$	$s_{1,-1}$	$t_{1,0}$	$t_{1,1}$	$t_{1,-1}$
100	1230	17.95	-0.89	0.94	-4.35	-3.65	1.10
200	2178	15.80	-0.85	2.41	-5.43	-3.24	1.41
300	1638	14.41	0.36	3.13	-5.95	-2.74	2.10
400	883	13.95	1.45	2.42	-5.65	-3.58	1.84
$S^2/No-KM-m_7$	3329	13.36	-0.09	1.05	-5.47	-1.52	2.08

to 11. Because Tycho-2 was used for the reduction of the 2MASS positions, we studied the surfaces of the B_T and V_T magnitudes in the neighborhood of the critical points. In a very general way the V_T surface mimics the extrema of the vector field, including the saddle points (these have not been included in the figures because we have selected only a few of them). It should be noted that the surface V_T is unique, while vector fields depend on the magnitude, spectral type and distance, showing patterns -in terms of singular points- different in each case.

Table 16. VSH coefficients for spectral types KM and m_4 magnitudes. 2MASS-Hip2. r means the center of the slice

$r=$	N	$s_{1,0}$	$s_{1,1}$	$s_{1,-1}$	$t_{1,0}$	$t_{1,1}$	$t_{1,-1}$
100	666	5.28	2.45	-5.94	15.70	1.94	0.04
200	1010	3.83	3.18	-6.80	19.58	2.31	0.81
300	618	1.94	5.29	-8.35	24.48	2.64	0.68
400	289	-0.23	10.75	-9.30	27.67	3.08	-0.71
500	118	2.62	14.54	-13.20	28.48	2.84	-6.84
$S^2/KM-m_4$	1402	4.68	4.12	-8.51	21.19	2.07	-0.99

Table 17. VSH coefficients for spectral types KM and m_5 magnitudes. 2MASS-Hip2. r means the center of the slice

$r=$	N	$s_{1,0}$	$s_{1,1}$	$s_{1,-1}$	$t_{1,0}$	$t_{1,1}$	$t_{1,-1}$
100	1179	6.45	4.15	0.38	3.37	1.09	2.97
200	3852	6.39	2.26	2.35	1.45	1.22	3.31
300	4744	6.85	0.94	2.72	1.38	1.01	3.51
400	3315	5.14	-0.25	1.22	3.66	-0.07	3.81
500	2263	0.72	0.33	-1.57	7.56	-1.70	2.81
$S^2/KM-m_5$	8186	4.46	0.48	0.68	5.22	-0.26	2.40

Table 18. VSH coefficients for spectral type KM and m_6 magnitudes. 2MASS-Hip2. r means the center of the slice

$r=$	N	$s_{1,0}$	$s_{1,1}$	$s_{1,-1}$	$t_{1,0}$	$t_{1,1}$	$t_{1,-1}$
100	769	11.84	-6.71	-3.29	8.14	6.32	5.98
200	1199	7.98	0.26	-0.60	2.21	4.01	4.38
300	3033	5.90	2.12	0.46	0.06	2.89	3.10
400	4081	4.85	2.71	1.48	0.56	2.25	2.47
500	3134	3.41	3.48	1.16	1.33	1.46	2.15
$S^2/KM-m_6$	6936	5.21	1.75	1.02	1.74	2.49	4.39

Table 19. VSH coefficients for spectral types KM and m_7 magnitudes. 2MASS-Hip2 r means the center of the slice. We only show the entries corresponding to the whole sphere because the slices correspomding to r=100, 200, 300, 400 and 500 pc contain only 402, 76, 74, 69 and 107 stars, respectively.

$r=$	N	$s_{1,0}$	$s_{1,1}$	$s_{1,-1}$	$t_{1,0}$	$t_{1,1}$	$t_{1,-1}$
$S^2/KM-m_7$	583	10.38	-5.33	-6.37	1.48	5.91	3.87

5.3. *Application to obtain some proper motions in the neighborhoods of the critical points*

In this subsection, we will consider some of the critical points obtained in the local study, selecting stars around the center within a radius of 0.2 rad. This will provide a number of stars common to Hipparcos and 2MASS in the neighborhood of the selected critical point for each case. We will choose some of them and we will apply the global correction depending on the spectral type of the star, its magnitude, and its distance according to TGAS. After these corrections, we follow an elementary process of position improvement (see (Marco et al. 2013) and (Michalik et al. 2014)). As the area of influence is small and we do not aim to obtain a joint solution (this issue will be considered in a further stage), it is not necessary to work with the positions in SMOK coordinates (Michalik et al. 2014). The quotient between the difference of positions (DR1 in t=2015 and improved version of 2MASS in t=2000) and the elapsed time for each star provides our approximation for the proper motions (see table 25) These values are compared with the

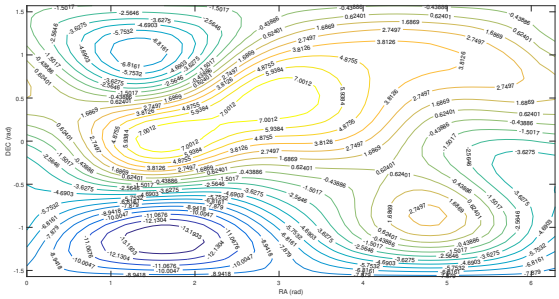

Figure 6. Contour lines corresponding to the potential of the [25, 200] pc slice..

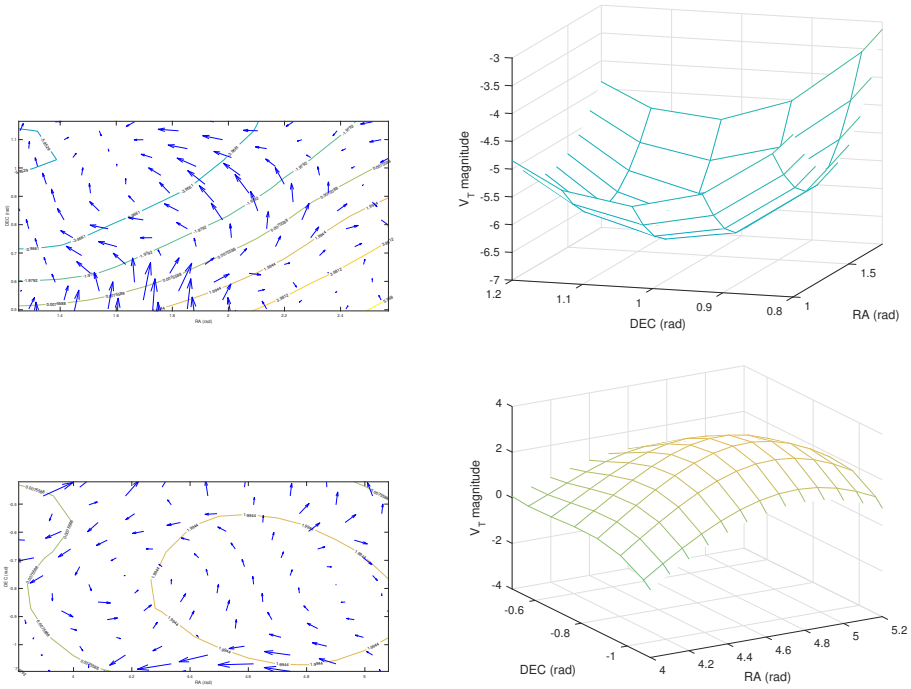

Figure 7. Slice 25-200. Up, Area III, $KM - m_5$, Shrink (1.6,1); Down, area I, $KM - m_4$, Sources (4.9,-0.8) (and (4.2,-0.75), its corresponding V_T surface is not shown) ; On the left, the potential vector field. On the right, the corresponding V_T surfaces.

¡

DR1 values and the PMA values which were obtained from DR1 and amelioration, using another procedure, from the 2MASS catalog. It must be taken into account that star-to-star comparisons are merely indicative. They cannot be representative, in a strict sense, because the adjustments for the elimination of bias are made by minimizing residuals in L^2-norm and not in L^∞-norm.

6. CONCLUSIONS

In this paper, we have presented a three-dimensional study of the vector field of positional residuals between 2MASS and Hipparcos-2, considering distances from TGAS provided in (Astraatmadja et al. 2016b). Such residuals have been used to obtain adjustments by nonparametric regression both for the entire sphere and for slices centered at the distances r = 100, 200,300, 400 and 500 pc. These regressions have been carried out so that we have obtained the vector fields at equally spaced points. This allows least squares adjustments from a continuous approach, using integrals, with the exception that these integrals are finally approximated by a numerical integration method. This procedure allows a robust evaluation of the desired parameters. In particular, the spheroidal and toroidal coefficients of the spherical vector harmonic developments that have been applied to vector fields. These have been computed for

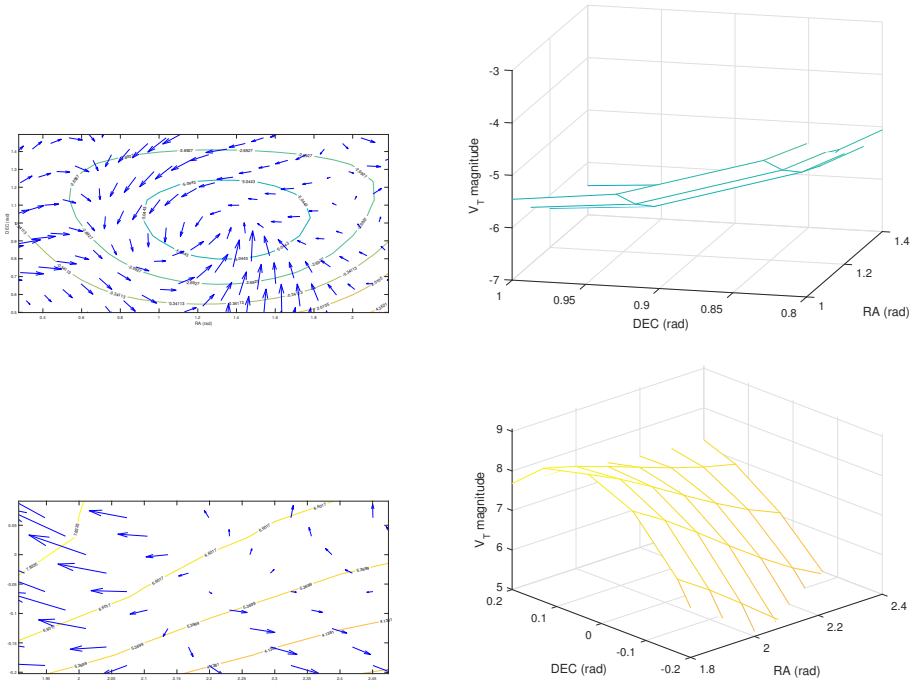

Figure 8. Slice 100-300. Up, area III, $KM - m_4$, Shrink (1.3,0.95); Down, area IV, $KM - m_5$, Source (2.2,0); On the left, the potential vector field. On the right, the corresponding V_T surface.

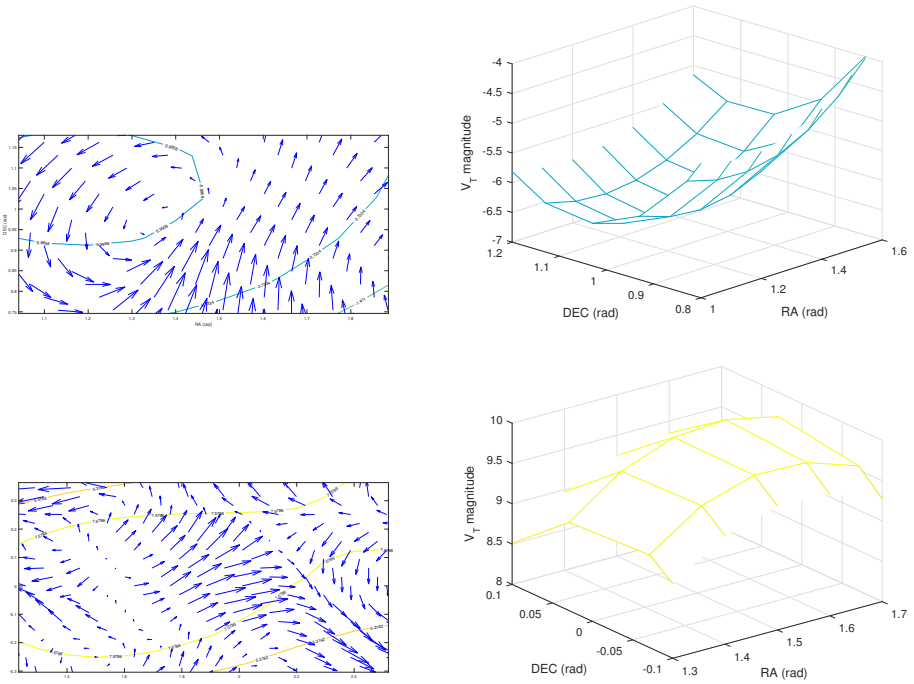

Figure 9. Slice 200-400; Up, area III, $KM - m_4$, Shrink (1.4,0.95); Down, area III, $KM - m_6$, Source (1.5,0.05); On the left, the potential vector field. On the right, the corresponding V_T surface.

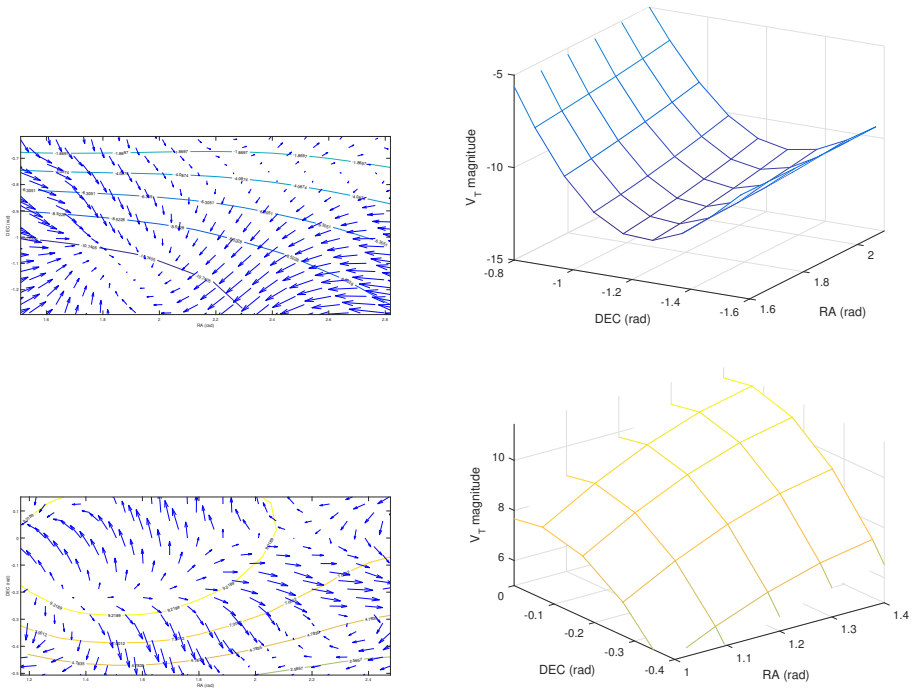

Figure 10. Slice 300-500. Up, area IV, $No - KM - m_5$, Shrink (1.85,-1.1). Down $No - KM - m_6$, area IV, Source (1.2,-0.2). On the left, the potential vector field. On the right, the corresponding V_T surface.

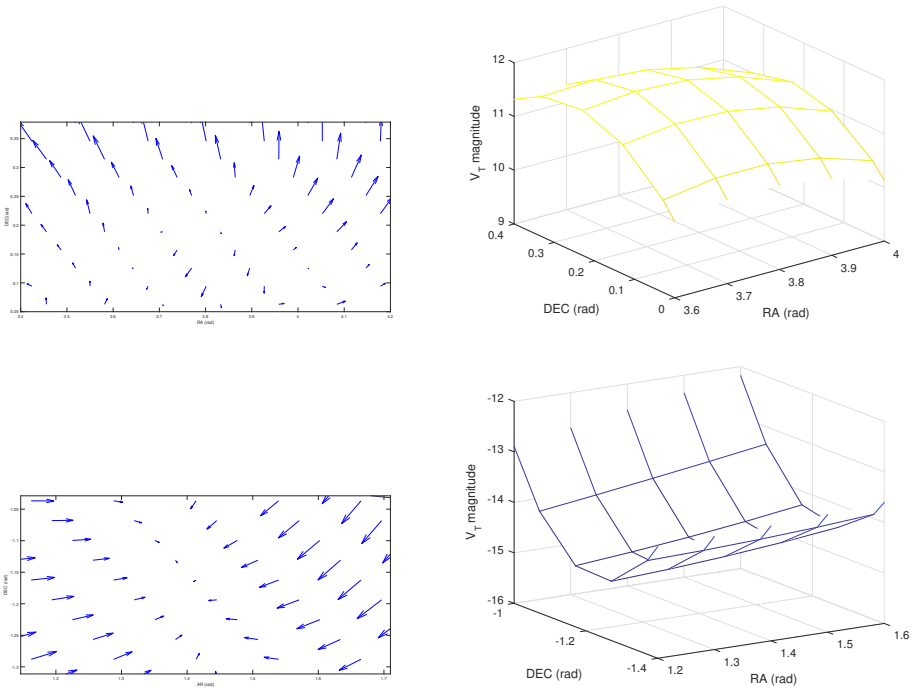

Figure 11. Slice 400-600 Up, area III, $KM - m_5$, Source (3,0.4); Down, area IV, $No - KM - m_6$, Shrink (1.4,-1.2); On the left, the potential vector field. On the right, the corresponding V_T surface.

Table 20. Singular points of the potential and the vector fields, classified by magnitudes, of the non-rotational component. *FS* means faint source, *AF* Attracting Focus

[25, 200)	Coordinates Type	m_4	m_5	m_6	m_7
I	4.7, −0.7) *Max*	*No − KM Source* (4.5, −1.05)	*Source* (4.6, −0.85)		*KM Source* (4.9, −0.8)
		No − KM Shrink (6.1, −1.15)			*KM Source* (4.2, −0.75)
II	(3.5, 0.5) *Max*	*No − KM Source* (3.9, 0.2)	*KM Source* (3.7, 0.45)	*KM Source* (4.4, 1)	
		No − KM Source (4.65, 0.92)			
III	(1.7, 0) *Max*	*KM Source* (2.3, 0.2)			(1.75, 0) *Source*
	(1.3, 1.05) *Min*	*No − KM Shrink* (0.85, 1.15)	*KM Shrink* (1.6, 1)	*KM Shrink* (0.4, 1.1)	*No − KM Source* (2.3, 0.5)
IV	(1.7, −1.1) *Min*	*KM Shrink* (2.47, −1.02)	*No − KM Shrink* (1.8, −1.15)	*KM Shrink* (1.9, −0.95)	
				No − KM Shrink (2, −1)	

several cases: a) all stars, not classified and classified by slices; b) taking into account if the stars are KM or Non-KM; c) According to four groups of H_p magnitudes that gather practically all of the stars; d) Idem with mixtures between KM and different magnitudes, and Non-KM and different magnitudes. We have verified how the coefficients of the vector fields depend on the spectral type and the magnitude, as well as on r. It should be noted that the adjustments have been made by "overlapping" and smoothly, so that the variations of the values of the parameters are also smooth, showing an (intuitive) idea of mathematical continuity. We stress that although the variations, between values of consecutive r, are small, they generally maintain a growing or decreasing tendency, with some exception.

To study the reliability of the results, case a) (see above) has been applied to 1000 samples created with perturbations times a N (0,1) for both AR and for DEC while for the distance has been considered a perturbation of the 10% of its value times a N(0,1). The results obtained for the real data are within the confidence interval for each coefficient, obtained by creating the perturbed data in the 1000 samples.

We have considered that the developments of first order for the toroidal component, are sufficient to determine the rotation between both catalogs. On the other hand, we have considered the non-rotational part of the field in more detail. To this aim, the Helmholtz Theorem has been used to decompose the vector field in its rotational part (the toroidal components of first order) and non-rotational. Focusing on the non-rotational part and considering that it is the gradient of a potential function, we deduce that the divergence of the residual field coincides with the Laplacian of the potential and that happens for each of the considered cases. If we assume that the potential can be developed in spherical (surface) harmonics, their properties lead immediately to the obtention of the Laplacian of such potential as the sum of coefficients (to be calculated) and the spherical functions themselves. The calculation of the divergence of the residual field is carried out by means of a polynomial local regression of first order, in order to obtain the first-order derivatives of each component and later the divergence of the vector field. The equality between both members allows,

Table 21. Singular points of the potential and the vector fields, classified by magnitudes, of the non-rotational component. *FS* means faint source, *AF* Attracting Focus

$[100, 300)$	Coordinates Type	m_4	m_5	m_6	m_7
I			*Shrink* $(5.7, -0.2)$	$No-KM$ *Source* $(4.7, -1.1)$	$(5.9, -0.2)$ *Shrink*
			Shrink $(5.4, 0.2)$		
II	$(3.1, 0.5)$ *Max*	KM *Shrink* $(2.8, 0.5)$		KM *Shrink* $(5.2, 0.1)$	$(2.7, 0.3)$ *Source*
		KM *Source* $(3.75, 0.82)$			
III	$(1.5, 0)$ *Max*	*Shrink* $(0.9, 1.1)$	KM *Shrink* $(1.15, 0.95)$		$No-KM$ *Source* $(2.2, 0)$
		KM *Shrink* $(1.3, 0.95)$			
	$(1.2, 1.1)$ *Min*				
IV	$(1.5, -1.25)$ *Min*	$No-KM$ *Source* $(1.5, -0.3)$	KM *Shrink* $(2, -1.10)$		$No-KM$ *Shrink* $(1.6, -1.25)$

through numerical integration, to obtain the coefficients of the potential. We verify that there are extrema for each potential that correspond to close critical points of the associated vector field. This happens, obviously, in areas of the sphere where the rotational component is small and, therefore, not very influential. From the results included in the tables of Section 5.2, it can be deduced that the patterns of the critical points and the potentials are dependents of r.

Finally, we have taken into account that the 2MASS reductions were made using the Tycho-2 as reference catalog. That is why we have studied the surfaces (here for the whole celestial sphere) corresponding to the magnitudes B_T and V_T. We have checked that for each critical point of each vector field (in which aspects such as the slice in which we works, the spectral type and the magnitude do have importance) there is a critical point of the V_T surface (the case of B_T, although in some cases could also be used, is, in general, less conclusive). In addition, there is a strong correspondence is between shrinks, sources and saddle points in the vector field and minimum, maximum and saddle points on the V_T surface (See figures from 8 to 12). With this and being aware that there are still questions to be answered, we have concluded our 2MASS-Hipparcos-2 residual analysis, is an apparently wide field of work that relates locally the geometry of vector fields to certain physical properties. Notice the importance, which can be seen in the tables and figures of Subsection 5.2, that the critical points of the surfaces of the magnitude V_T are obtained considering the complete celestial sphere, while their relative extrema correspond to critical points of residual vector fields corresponding to a specific subgroup of stars and a certain distance. This confirms the importance of the 3D study introduced/studied in this article.

It is interesting to note that three issues remain. Firstly is the search for a classification by statistical clusters, taking into account at least distances, spectral types, and magnitudes. Secondly, the improved recent massive catalogs with which to compare different aspects of the Gaia Data Release that are to appear. And thirdly, the Helmholtz decomposition of the velocity field of a catalog, studying the potentials in the different cases in which this vector field is found and seeing the possible implications of the obtained results. It is clear that these issues are to be addressed in later work.

Table 22. Singular points of the potential and the vector fields, classified by magnitudes, of the non-rotational component. FS means faint source, AF Attracting Focus, SF Source Focus

$[200, 400)$	Coordinates Type	m_4	m_5	m_6	m_7
I		KM $Source$ $(5.9, -0.45)$		KM $Shrink$ $(5.1, 0)$	$Shrink$ $(6.1, -0.1)$
		$Shrink$ $(5.7, 0)$			$No-KM$ $Shrink$ $(5.9, -0.3)$
		$No-KM$ $Shrink$ $(5.6, -0.1)$			
II		KM $Source$ $(4.8, 0)$		$No-KM$ $Shrink$ $(5.5, 1.05)$	$Source$ $(1.9, -0.05)$
					$No-KM$ $Source$ $(1.9, -0.05)$
III	$(1.2, 1.1)$ Min	KM $Shrink$ $(1.4, 0.95)$	$No-KM$ $Shrink$ $(1.4, 1.2)$	KM $Shrink$ $(1.1, 1.15)$	
		$Shrink$ $(1.2, 0.85)$			
	$F_1(1.5, 0)$ Max		$Shrink$ $(1.4, 1.5)$	KM $Source$ $(1.5, 0.05)$	
	$F_1(3, 0.25)$ Max		KM $Source$ $(1.3, 0)$		
			$Source$ $(1.7, -0.15)$		
IV	$(1.5, -1.25)$ Min		$No-KM$ $Shrink$ $(1.7, -1.2)$		$No-KM$ $Shrink$ $(1.5, -1.25)$
			$Shrink$ $(1.8, -1)$		

After a simple process of local improvement of the 2MASS stars located in the neighborhood of some of the singular points that appeared in Subsection 5.2, we have applied the adjustments obtained in Subsection 5.1 to deduce the induced proper motions and compare them with those provided by DR1 and PMA. It must be neared in mind that the local corrections have not been arranged in the way of a search for a joint solution and that the adjustments we use to minimize the L^2-norm, so that the comparison one by one, that is, in the L^∞-norm, should be done with caution and the results are merely indicative.

ACKNOWLEDGEMENTS

This paper was partially supported by the UJI-B2016-18, 16I356 project.

REFERENCES

Akhmetov et al. The PMA Catalog: 420 million positions and absolute proper motions, MNRAS 469, 763-773 (2017)

Arenou et al. Gaia Data Release 1: Catalogue validation, A&A 599, A50 (2017)

Table 23. Singular points of the potential and the vector fields, classified by magnitudes, of the non-rotational component. *FS* means faint source, *AF* Attracting Focus, *SF* Source Focus

$[300, 500)$	Coordinates Type	m_4	m_5	m_6	m_7
I	$(5.9, 0)$ Min	$Shrink$ $(5.8, -0.05)$	$Shrink$ $(5.8, -0.1)$		$Shrink$ $(5.8, -0.1)$
II	$(3.4, 0)$ $Max\ rel$				
III	$(0.5, 1)$ Min	KM $Shrink$ $(2.95, 0.35)$	$No-KM$ $Shrink$ $(5.1, 1.2)$	$Shrink$ $(0.1, 1.23)$	
	$(1.5, 0)$ Max			KM $Source$ $(1.6, 0.1)$	$Source$ $(1.9, -0.1)$
IV	$(1, -1.25)$ Min		$No-KM$ $Shrink$ $(1.85, -1.10)$	$No-KM$ $Source$ $(1.2, -0.2)$ $No-KM$ $Shrink$ $(1.4, -1.2)$ $No-KM$ $Source$ $(2.5, -0.3)$	$No-KM$ $Source$ $(1.8, -0.1)$

Table 24. Singular points of the potential and the vector fields, classified by magnitudes, of the non-rotational component. *FS* means faint source, *AF* Attracting Focus, *SF* Source Focus

$[400, 600)$	Coordinates Type	m_4	m_5	m_6	m_7
I					
II	$(3.7, 0.3)$ Max		KM $Source$ $(3, 0.4)$	KM $Source$ $(3.8, 0.2)$	
III	$(0.25, 1)$ Min				
	$(1.7, 0)$ Max				$Source$ $(1.9, -0.05)$
IV	$(1, -1.25)$ Min			$No-KM$ $Shrink$ $(1.4, -1.2)$	$No-KM$ $Shrink$ $(1.5, -0.9)$

Table 25. Comparison between the proper motions from DR1, PMA and our obtained results for some stars in the neighborhood of some singular points of their vector field. Hip stands for the number of the star in the Hipparcos catalogue, DR1 for the DR1 identifier. Subindex (1) means $DR1$ and (2) means PMA. The proper motions are given in mas, being the last two colums μ^*_α μ_δ our obtained results.

Hip	$DR1$	$\alpha_{(1)}$	$\delta_{(1)}$	$\mu^*_{\alpha\,(1)}$	$\mu_{\delta\,(1)}$	$\mu^*_{\alpha\,(2)}$	$\mu_{\delta\,(2)}$	μ^*_α	μ_δ
28951	1008018207212849024	91.6628127275	63.4538738263	−35.558	8.594	−34.73	21.84	−36.35	21.33
30031	998050069154382592	94.7912065760	56.5264619828	−37.640	−31.332	–	–	−39.10	−31.05
24771	188796557490084480	79.6695937289	−32.3228506874	4.963	−13.891	3.08	−20.75	4.47	−23.68
27047	4756115082715073920	86.0379453784	−65.1018594755	−2.259	21.541	−4.01	26.0	−2.24	27.01
23865	279443525899748352	76.9426318743	55.7590984639	26.115	−14.343	22.01	−16.58	29.28	−21.70
89345	6721441368029854976	273.4528707722	−43.2043919512	−9.007	−13.989	−8.55	−17.27	−9.91	−18.69
44931	3841861165533628672	137.2857737710	−1.5880525106	−27.981	−35.349	−28.80	−45.08	−23.34	−43.16
23863	279443525899748352	76.9426318743	55.7590984639	26.115	−14.3434	22.01	−16.58	28.47	−22.17

Astraatmadja, Tri I. and Bailer-Jones, A.L., 2016a. Estimating distances from paralaxes. II. Performance of bayesian distance estimators on Gaia-like Catalogue. The Astrophysical Journal 832: 137

Astraatmadja, Tri I. and Bailer-Jones, A.L., 2016b. Estimating distances from paralaxes. III. Distances of two million stars in the Gaia DR1 Catalogue. The Astrophysical Journal 833, N. 1: 119

Bailer-Jones, C. A. L. 2015, Estimating distances from parallaxes, PASP, 127, 994

Bien, R., Fricke, W., Lederle, T., & Schwan, H. 1978, The construction of the Fifth Fundamental catalog (FK5), Vero . Astron. Rechen-Inst. Heidelberg, No. 2

Brosche P. 1966. Representation of systematic differences in positions and proper motions of stars by spherical harmonics. Vero . Astron. Rechen-Inst. Heidelberg, No. 17

Brown, A. G. A., et al. 2016, Gaia Data Release 1. Summary of the astrometric, photometric, and survey properties (Gaia Collaboration) A&A, 595, A2

Brown, A. G. A., et al. 2018, (Gaia Collaboration) A&A, (In Press)

Cutri, R. M., et al. 2003, 2MASS All Sky Catalog of point sources. The IRSA 2MASS All-Sky Point Source Catalog, NASA/IPAC Infrared Science Archive.

Fan, J. and Gijbels,I. 1996. Local Polynomial Modelling and Its Applications: Monographs on Statistics and Applied Probability 66. Chapman and Hall

Copenhagen Univ. Obs. Inst. of Astronomy, Cambridge, UK & Real Instituto y Observatorio de la Armada, F.E.S., 2016. CMC14, Vizier Online data Catalog 1304, 0

Davies G.R. et al. 2017, Systematic error of the Gaia DR1 TGAS Parallaxes from data for the Read Giant Clump, AA 598, L4.

Gontcharov G.A. 2017, Systematic error of the Gaia DR1 TGAS Parallaxes from data for the Read Giant Clump, Astronomy Letters, 43(8)

Heiskanen W. and Moritz H., 1967, Physical Geodesy, Ed. W.H. Freeman and Company.

Høg, E., Fabricius, C., Makarov, V. V., et al. 2000, The Tycho-2 catalogue of the 2.5 million brightest stars, A&A, 355, L27

Jeffreys, H., 1967 A Completeness Theorem for Expansions of a Vector Function in Spherical Harmonics , Geophys. J. R. astr. SOC. 12,: 465

Lindegren, L., Lammers, U., Hobbs, D., et al. 2012, The astrometric core solution for the Gaia mission. Overview of models, algorithms, and software implementation (the AGIS paper) A&A, 538, A78

Lindegren, L., Lammers, U., Bastian, U., et al. 2016, Data Gaia Release 1. Astrometry: one billion positions, two million proper motions and parallaxes, A&A, 595, A4

Makarov V.& Murphy D.W. 2007, The Local Stellar Velocity Field Via Vector Spherical Harmonics, AJ 134 (1)

Marco, F.J. et al., 2004. A critical discussion on parametric and nonparametric regression methods applied to Hipparcos-FK5 residuals, A&A 418, N.3: 1119

Marco, F.J. et al., 2013. Homogenization in compiling ICRF combined catalogs, A&A 558, A98

Marco, F.J. et al., 2015. Application of Vector Spherical Harmonics and Kernel Regression to the Computations of OMM Parameters, AJ 149, N. 4: 129

Masry, E. and Fan, J. Local, 1997. Polynomial Estimation of Regression Functions for Mixing Processes. Scandinavian Journal of statistics 24, N. 2: 165

Michalik et al., 2014, Joint astrometric solution of HIPPARCOS and Gaia — A recipe for the Hundred Thousand Proper Motions project, A&A, 571, A85

Michalik, D., Lindegren, L., & Hobbs, D. 2015, The Tycho-Gaia astrometric solution. How to get 2.5 million parallaxes with less than one year of Gaia data. A&A, 574, A115

Michalik, D., & Lindegren, L. 2016, Quasars can be used to verify the parallax zero-point of the Tycho-Gaia Astrometric Solution, A&A, 586, A26

Mignard, F. & Morando B., 1990. Analyse de catalogues stellaires au moyen des harmoniques vectorielles, Journées 1990: Systèmes de référence spatio-temporels, p. 151

Mignard, P., 2000, Local galactic kinematics from Hipparcos proper motions, A&A 354: 522

Mignard, F. & Klioner, S. 2012 . Analysis of astrometric catalogues with vector spherical harmonics A&A 547, A59

Morse, P.C. & Feshback, H., 1953, Methods of Theoretical Physics, McGraw - Hill

Perryman, M. A. C. & ESA, eds. 1997, ESA Special Publication, Vol. 1200,The HIPPARCOS and TYCHO catalogues. Astrometric and photometric star catalogues derived from the ESA HIPPARCOS Space Astrometry Mission

Prusti T. et al. 2016 The Gaia mission (Gaia Collaboration) A&A 595, A1

Ridder et al. 2016. Asteroseismic versus Gaia distances: a first comparison. A&A 595, L3

Röser, S. and Bastian, U., 1991 PPM Star Catalogue, Heidelberg (New York: Published for Astronomisches rechen-Institut by Spectrum Akademischer Verlag)

Röser et al., 2008, PPM - Extendeed (PPMX) - a catalogue of positions and proper motions, A&A 488

Röser et al., 2010, The PPMXL catalog of positions and proper motions on the ICRS. Combining USNO B1.0 and the Two Micron All Sky Survey, AJ 139, N. 6: 2440

Schönrich R. & Aumer M., 2017, Assesing distances and consistency of kinematics in Gaia/TGAS, MNRAS, 472, 4

Schwann, H., 2001 An analytical representation of the systematic differences HIPPARCOS-FK5, A&A 367:1078

Skrutskie M.F et al, 2006, The Two Micron All Sky Survey (2MASS), AJ 131, N. 2: 1163

Simonoff, J.S., 1996. Smoothing Methods in Statistics. Springer

Stassun K.G. & Torres G., 2016, Evidence for a systematic error offset of -0.25 mas in the Gaia DR1 parallaxes, The Astrophysical Journal Letters, 831:L6

Urban, S.E., 2001 The AC 2000.2 Catalogue

van Leeuwen, F. 2007a, Validation of the new Hipparcos reduction, A&A, 474, 653

van Leeuwen, F. 2007b, Hipparcos, the New Reduction of the Raw Data (Springer), Astrophys. Space Sci. Libr., 350 (Vizier Online data Catalog I/311/hip2)

Vityazev, V.V and Tsevtkov, A.S., 2009, Analysis of the three-dimensional stellar velocity field using vector spherical functions, Astronomy Letters 35, N. 2: 100

Vityazev, V.V. et al., 2011, Application of vector spherical harmonics for kinematic analysis of stars from zonal catalogues, Astronomy Letters 37, N.12 :874

Vityazev, V.V and A.S. Tsvetkov, 2013, UCAC4: Stellar kinematics with vector spherical functions, Astron. Nachr. 334, N. 8: 760

Vityazev, V.V. and Tsevtkov, A.S., 2014. Intercomparison of kinematics derived from catalogues UCAC4, PPMXL and XPM with vector spherical harmonics, MNRAS 442, N. 2: 1249

Vityazev, V.V. and Tsevtkov, A.S., 2015. Systematics Differences between the positions and proper Motions of Stars from the PPMXL and UCAC4 Catalogs, Astronomy letters 45, N. 7: 317

Vityazev, V.V. et al., 2017a. Comparison of XPM and UCAC4 catalogues in the galactic coordinate system, Astron. Nachr 338, N. 4: 489

Vityazev, V.V and A.S. Tsvetkov, 2017b, Properties of the Tycho-2 Catalogue from Gaia Data Release, Astronomy letters 43, N. 11: 730

Vityazev et al. 2017c, Galactic kinematics derived from data in the RAVE5, UCAC4, PPMXL, AND Gaia TGAS Catalogs, Astrophysics 60, N. 4: 503

Wand, M.P. and Jones M.C., 1995 Kernel Smoothing. Monographs on Statistics and Applied Probability 60. Chapman and Hall

Wielen et al., 2001, PThe Astrometric Catalog ARIHIP, Veroeff. Astron, Rechen-Inst. Heidelberg, Vol. 40 :1-36

Zacharias N. et al., 2000, The first USNO astrograph catalog. AJ 120: 2131

Zacharias N. et al., 2004, The Second US Naval Observatory CCD Astrograph Catalog (UCAC2). AJ 127, N. 5: 3043

Zacharias N. et al., 2013, The Fourth US Naval Observatory CCD Astrograph Catalog (UCAC4), AJ 145, N. 2: 44

Zacharias N. et al., 2017, UCAC5: New Proper Motions using Gaia DR1, AJ 153, N. 4: 166

Zinn J.C. et al., 2017, Evidence for spatially-correlated Gaia parallax errors in the Kepler field, AJ, 844, N. 2

APPENDIX

A. SURFACE SPHERICAL HARMONICS

We present in this Annex the surface spherical harmonics up to 5th order:

$Y_{00}(\sin\delta) = 1$
$Y_{10}(\sin\delta) = \sin\delta$
$Y_{1,-1}(\sin\delta) = \cos\delta\cos\alpha$
$Y_{1,1}(\sin\delta) = \cos\delta\sin\alpha$
$Y_{2,-2}(\sin\delta) = 3\cos^2(\delta)\cos(2\alpha)$
$Y_{2,-1}(\sin\delta) = 3\sin\delta\cos(\delta)\cos(\alpha)$
$Y_{2,0}(\sin\delta) = \frac{3}{2}\sin\delta\sin(\delta) - \frac{1}{2}$
$Y_{2,1}(\sin\delta) = 3\sin\delta\cos(\delta)\sin(\alpha)$
$Y_{2,2}(\sin\delta) = 3\cos^2(\delta)\sin(2\alpha)$
$Y_{3,-3}(\sin\delta) = 15\cos^3(\delta)\cos(3\alpha)$
$Y_{3,-2}(\sin\delta) = 15\sin\delta\cos^2(\delta)\cos(2\alpha)$
$Y_{3,-1}(\sin\delta) = \frac{3}{2}\left(5\sin^2\delta - 1\right)\cos(\delta)\cos(\alpha)$
$Y_{3,0}(\sin\delta) = \frac{1}{2}\left(5\sin^3\delta - 3\sin(\delta)\right)$
$Y_{3,1}(\sin\delta) = \frac{3}{2}\left(5\sin^2\delta - 1\right)\cos(\delta)\sin(\alpha)$
$Y_{3,2}(\sin\delta) = 15\sin\delta\cos^2(\delta)\sin(2\alpha)$
$Y_{3,3}(\sin\delta) = 15\cos^3(\delta)\sin(3\alpha)$
$Y_{4,-4}(\sin\delta) = \cos^4(\delta)\sin(4\alpha)$
$Y_{4,-3}(\sin\delta) = \sin\delta\cos^3(\delta)\sin(3\alpha)$
$Y_{4,-2}(\sin\delta) = 7\left(\sin^2\delta - 1\right)\cos^2(\delta)\sin(2\alpha)$
$Y_{4,-1}(\sin\delta) = \sin\delta\left(7\sin^2\delta - 3\right)\cos(\delta)\sin(\alpha)$
$Y_{4,0}(\sin\delta) = 35\sin^4\delta - 30\sin^2(\delta) + 3$
$Y_{4,1}(\sin\delta) = \sin\delta\left(7\sin^2\delta - 3\right)\cos(\delta)\cos(\alpha)$
$Y_{4,2}(\sin\delta) = 7\left(\sin^2\delta - 1\right)\cos^2(\delta)\cos(2\alpha)$
$Y_{4,3}(\sin\delta) = \sin\delta\cos^3(\delta)\cos(3\alpha)$
$Y_{4,4}(\sin\delta) = \cos^4(\delta)\cos(4\alpha)$
$Y_{5,-5}(\sin\delta) = \sin^5(\delta)\sin(5\alpha)$
$Y_{5,-4}(\sin\delta) = \sin\delta\cos^4(\delta)\sin(4\alpha)$
$Y_{5,-3}(\sin\delta) = \left(9\sin^2\delta - 1\right)\cos^3(\delta)\sin(3\alpha)$
$Y_{5,-2}(\sin\delta) = 3\left(\sin^3\delta - \sin\delta\right)\cos^2(\delta)\sin(2\alpha)$
$Y_{5,-1}(\sin\delta) = \cos\delta\left(21\sin^4\delta - 14\cos^2(\delta) + 1\right)\sin(\alpha)$
$Y_{5,0}(\sin\delta) = 63\sin^5\delta - 70\sin^3\delta - 14\cos^2(\delta) + 15\sin\delta$
$Y_{5,1}(\sin\delta) = \cos\delta\left(21\sin^4\delta - 14\cos^2(\delta) + 1\right)\cos(\alpha)$
$Y_{5,2}(\sin\delta) = 3\left(\sin^3\delta - \sin\delta\right)\cos^2(\delta)\cos(2\alpha)$
$Y_{5,3}(\sin\delta) = \left(9\sin^2\delta - 1\right)\cos^3(\delta)\cos(3\alpha)$
$Y_{5,4}(\sin\delta) = \sin\delta\cos^4(\delta)\cos(4\alpha)$
$Y_{5,5}(\sin\delta) = \sin^5(\delta)\cos(5\alpha)$

B. SPHEROIDAL AND TOROIDAL SPHERICAL HARMONICS USED

We include a list of the Spheroidal and Toroidal spherical harmonics used in this paper. The general formulation may be seen in Morse & Feshback (1953) . For clarity, we have not included the norms in these formulas.

$$
\begin{aligned}
S_{1,-1} &= -\cos l\,\overrightarrow{e}_l + \sin l \sin b\,\overrightarrow{e}_b \\
S_{1,0} &= \cos b\,\overrightarrow{e}_b \\
S_{1,1} &= \sin l\,\overrightarrow{e}_l + \cos l \sin b\,\overrightarrow{e}_b \\
S_{2,-2} &= 6\cos 2l \cos b\,\overrightarrow{e}_l - 6\sin 2l \cos b \sin b\,\overrightarrow{e}_b \\
S_{2,-1} &= -3\cos l \sin b\,\overrightarrow{e}_l - 3\sin l \cos 2b \sin b\,\overrightarrow{e}_b \\
S_{2,0} &= 3\cos b \sin b\,\overrightarrow{e}_b \\
S_{2,1} &= 3\sin l \sin b\,\overrightarrow{e}_l - 3\cos l \cos 2b\,\overrightarrow{e}_b \\
S_{2,2} &= -6\sin 2l \cos b\,\overrightarrow{e}_l - 6\cos 2l \cos b \sin b\,\overrightarrow{e}_b \\
S_{3,-1} &= -\left(5\sin^2 b - 1\right)\cos l\,\overrightarrow{e}_l + \sin l \sin b\left(15\sin^2 b - 11\right)\overrightarrow{e}_b \\
S_{4,2} &= \left(7\sin^2 b - 1\right)\cos b \sin 2l\,\overrightarrow{e}_l + \left(7\sin^2 b - 4\right)\sin 2b \cos 2l\,\overrightarrow{e}_b
\end{aligned}
\tag{B1}
$$

$$
\begin{aligned}
T_{1,-1} &= \sin l \sin b\,\overrightarrow{e}_l + \cos l\,\overrightarrow{e}_b \\
T_{1,0} &= \cos b\,\overrightarrow{e}_l \\
T_{1,1} &= \cos l \sin b\,\overrightarrow{e}_l - \sin l\,\overrightarrow{e}_b \\
T_{2,-2} &= -6\sin 2l \cos b \sin b\,\overrightarrow{e}_l - 6\cos 2l \cos b\,\overrightarrow{e}_b \\
T_{2,-1} &= -3\sin l \cos 2b\,\overrightarrow{e}_l + 3\cos l \sin b\,\overrightarrow{e}_b \\
T_{2,0} &= 3\cos b \sin b\,\overrightarrow{e}_l \\
T_{2,1} &= -3\cos l \cos 2b\,\overrightarrow{e}_l - 3\sin l \sin b\,\overrightarrow{e}_b \\
T_{2,2} &= -6\cos 2l \cos b \sin b\,\overrightarrow{e}_l + 6\sin 2l \cos b\,\overrightarrow{e}_b
\end{aligned}
\tag{B2}
$$